Research Square

Preprints are preliminary reports that have not undergone peer review.
They should not be considered conclusive, used to inform clinical practice,
or referenced by the media as validated information.

Magnetic Biochar Interfaces: Tuning Surface Functionality via Green Activation Methods for Environmental Cleanup

D. Jayarajan
Assam down town University
S. Sivaprakash
St. Joseph's College of Arts and Science (Autonomous)
R. Sagayaraj
sagayaraj@sjctnc.edu.in

St. Joseph's College of Arts and Science (Autonomous)

Systematic Review

Keywords: magnetic biochar, green activation, surface functional groups, iron oxides, persistent free radicals, adsorption, advanced oxidation, sustainable materials

Posted Date: November 24th, 2026

DOI: https://doi.org/10.21203/rs.3.rs-11745826/v1

License: This work is licensed under a Creative Commons Attribution 4.0 International License.
Read Full License

Additional Declarations: No competing interests reported.

Magnetic Biochar Interfaces: Tuning Surface Functionality via Green Activation Methods for Environmental Cleanup

D. Jayarajan[1], S. Sivaprakash [2], R. Sagayaraj[3],*

[1]Program of MLS, Faculty of Allied and Healthcare Sciences, Assam down town University, Sankar Madhab Path, Gandhi Nagar, Panikhaiti, Guwahati, Assam, India, PIN – 781026

[2]PG & Research Department of Zoology, St. Joseph's College of Arts and Science (Autonomous), Cuddalore-607001, Affiliated to Annamalai University, Tamil Nadu, India

[3]PG & Research Department of Physics, St. Joseph's College of Arts and Science (Autonomous), Cuddalore-607001, Affiliated to Annamalai University, Chidambaram, Tamil Nadu, India

Abstract

Magnetic biochar (MBC) combines the porous, functional-group-rich surface of pyrolytic carbon with the magnetic recoverability of iron-based nanophases, but its performance is set at three coupled interfaces: the solid–liquid surface, the carbon–iron junction and the pore–mineral boundary. Conventional routes to high-performance MBC (strong bases, chlorinated iron salts, large wash volumes, high-temperature furnaces) conflict with the sustainability rationale of biochar. This review examines 94 sources published between 2021 and 2026 and relates "green" activation and magnetization strategies (steam and CO_2 activation, mild and bio-derived chemical activation, plant-extract iron synthesis, waste-derived iron, microwave, hydrothermal, mechanochemical, low-temperature carbothermal and electrochemical routes) to the surface chemistry, iron speciation and porosity they produce, and then to the mechanisms that govern pollutant removal. Fourteen figures and nine tables synthesize the evidence. Representative reported values illustrate the range of outcomes. Cr(VI) removal rose from 61.42% (pristine biochar) to 72.37% (magnetic) and 100% (bifunctionalized magnetic biochar) in one rice-straw system. A low-temperature (400 °C) potassium ferrate/NaOH carbothermal route gave zero-valent-iron-doped biochar with a saturation magnetization of 56.3 emu g^{-1} and capacities of 1106.25 mg g^{-1} for tetracycline and 182.03 mg g^{-1} for ciprofloxacin. Ball-milled magnetic cotton-husk biochar reached 266.7 mg g^{-1} for oxytetracycline, 1.6 times that of unmodified biochar. Iron doping raised environmental persistent free radical content from 3.33 to 9.11 × 10^{18} spins g^{-1} in one hydrochar, yet excess iron lowered it from 7.95 to 2.78 × 10^{18} in another, and magnetite activation reduced Pb(II) uptake by up to 86% in some biochars. Oxidant activation typically proceeds through coexisting radical and non-radical pathways (about 56% and 44%,

respectively, in a red-mud biochar). Regeneration is often incomplete (61.12% removal retained after five cycles in one case, 83–86% in others), and electricity was the dominant life-cycle hotspot (5.44 kg CO_2-eq per kg of a microwave-modified adsorbent). Key knowledge gaps are non-standard interfacial characterization, scarce real-water and iron-leaching data, and small datasets for machine learning. We propose a five-step design and assessment roadmap for scalable, low-impact magnetic biochar interfaces.

Keywords: magnetic biochar; green activation; surface functional groups; iron oxides; persistent free radicals; adsorption; advanced oxidation; sustainable materials

Corresponding author: R. Sagayaraj (sagayaraj@sjctnc.edu.in)

1. Introduction

Biochar, the carbon-rich solid produced by pyrolysis of biomass under oxygen-limited conditions, has become a versatile platform material for environmental cleanup because of its low cost, waste-derived feedstocks, tunable porosity and surface functional groups [1–3]. Pristine biochars nevertheless face two practical limits in water treatment: modest capacity for anionic species and difficult recovery of fine particles. Magnetization addresses the second limit by impregnating or growing ferromagnetic or ferrimagnetic phases on or within the carbon matrix [1, 2], and recent reviews report that magnetized biochars offer higher adsorption capacity and better reusability than their non-magnetic precursors [3]. For antibiotics, reported capacities of magnetic biochar range from about 5 to 900 mg g^{-1}, and most materials remove over 90% within 60 min [4].

Magnetization is also an interfacial modification. Iron functionalization introduces binding and redox sites and changes how the carbon surface exchanges electrons with contaminants and oxidants, so that iron–carbon interactions govern adsorption, redox activity and electron transfer [5]. Engineered magnetic biochars that combine metals and functional groups with magnetic nanoparticles, for example by ultrasonic- or microwave-assisted routes, extend this concept to selective removal of heavy metals and organics [6]. Biochar-borne persistent free radicals and redox-active moieties take part in catalytic oxidation [7–9], and magnetic biochar has been shown to raise the electron transfer capacity of the material in microbial systems [10].

The routes most often used to make these materials, however, carry environmental costs. Direct hydrothermal synthesis has attracted attention because of its mild conditions [3]. Physical modifications such as steam activation, heat treatment and ball milling increase porosity and

surface area without chemical activating agents [5, 11], and green-chemistry syntheses using low-cost iron precursors are making iron-modified biochar more sustainable [5]. Plant-extract-mediated synthesis has been used to introduce magnetic iron nanoparticles into biochar [12, 13], industrial and sewage wastes have served as iron and carbon sources [14, 15], and milder activators such as K_2CO_3 and oxidative iron salts such as K_2FeO_4 are replacing harsher reagents [16–18]. Despite this progress, long-term stability against iron leaching, regeneration and environmental risk remain open questions [4, 5].

Magnetic biochar is also being evaluated beyond water treatment. Recent reviews examine its preparation and the microbiological response when it is applied to soils polluted with heavy metals [19], and mineral-enriched biochar has been shown to deliver improved nutrient recovery and carbon dioxide removal [20]. In parallel, machine learning is beginning to guide biochar preparation and predict adsorption [21–23], and life-cycle assessments of magnetic-biochar-based processes and of hydrochar-embedded magnetic nanoparticles are emerging [24, 25].

In this review we use "green activation" to mean activation and magnetization strategies that (i) reduce or replace hazardous, corrosive or persistent reagents, (ii) lower energy and water demand, (iii) valorize waste or bio-derived inputs, and (iv) limit secondary pollution such as iron leaching or toxic effluents, without sacrificing functional performance. Because the topic falls within surface science, the discussion is organized around interfaces: how each route tailors the carbon surface, the carbon–iron junction and the solid–liquid boundary, and how those features translate into mechanisms and measured performance. Literature was restricted to publications from 2021 to 2026, identified through targeted searches of publisher and indexing platforms; entries for which only partial bibliographic data could be retrieved are flagged in the reference list. Section 2 summarizes the fundamentals of magnetic biochar interfaces. Section 3 reviews green activation and magnetization routes. Section 4 links processing to surface functionality. Section 5 analyzes interfacial mechanisms. Section 6 presents a comparative analysis of reported performance. Section 7 discusses stability, sustainability and data-driven design, and Sections 8 and 9 give an outlook and conclusions.

2. Fundamentals of Magnetic Biochar Interfaces

2.1 Feedstock, pyrolysis and the carbon scaffold

The carbon scaffold inherits its composition from the feedstock and is shaped by pyrolysis temperature, heating rate and residence time. Agricultural residues such as rice straw, tea residue

and sludges are frequent feedstocks, and overviews of rice-straw biochar production link process conditions to wastewater-remediation performance [26]. Tea residue has been pyrolyzed and loaded with Fe_3O_4 by impregnation–coprecipitation to give a heterogeneous catalyst with measurable magnetic properties [27], whereas sewage, pharmaceutical and Fenton sludges and red mud have been used to supply both carbon and iron [14, 15, 28]. Walnut-shell biochar has been characterized together with magnetized variants at decreasing iron content, which allows saturation magnetization to be related to iron loading [29]. Generally, higher pyrolysis temperatures increase aromaticity, graphitization and porosity while removing acidic surface groups [30, 31], so feedstock and temperature must be matched to the intended interfacial function.

2.2 Magnetic phases and their roles

The magnetic response of MBC arises from iron-containing phases whose identity determines both recoverability and chemical function (Table 1). Nanoscale reduced iron is notably prone to oxidation, which complicates preparation of stable particles [32].

Table 1. *Magnetic and iron-containing phases reported for magnetic biochars and their interfacial roles.*

Phase / system	Reported interfacial role	Main concern	Ref.
Magnetite (Fe_3O_4) on biochar	Fe(II)/Fe(III) cycling for peroxymonosulfate (PMS) activation; magnetic recovery verified by VSM	Agglomeration and ion leaching of bare nanoparticles	[3, 27, 28]
Zero-valent iron (ZVI), including S-doped nZVI	Reductive and sorptive removal of phosphorus and antibiotics	Oxidation of Fe^0	[17, 32, 33]
Spinel ferrite ($MnFe_2O_4$@BC)	Coexisting radical and non-radical PMS activation	Secondary-metal leaching	[34]
Goethite / biochar	Radical and non-radical tetracycline degradation	Lower magnetic response than magnetite	[35]
Iron nitride (Fe_xN) in pharmaceutical-sludge	Endogenous Fe plus exogenous N doping enhances PMS activation	Heterogeneous waste feedstock	[15]

biochar			
Cu-doped magnetic biochar	Enhanced PMS activation for sulfamethoxazole degradation	Cu release	[36]
Mg–Fe layered double hydroxide on Fe_3O_4 biochar	Anion exchange (phosphate) with magnetic recovery (2.63 emu g^{-1})	Low saturation magnetization	[37]
Graphene-encapsulated Fe^0 (BC-G@Fe^0)	Heavy-metal uptake; carbon shell protects reduced iron	Hard-to-control carbothermal reduction	[38]

2.3 Three interfaces that matter

Three coupled interfaces can be engineered to some degree independently (Figure 1). At the solid–liquid interface, protonation, double-layer formation, ion exchange and complexation determine uptake; in bifunctionalized magnetic biochar, added amino and sulfur functionalities and Fe(II) contribute to Cr(VI) reduction and electrostatic attraction [39]. At the carbon–iron interface, strong coupling can stabilize particles, enable electron transfer and enhance electron transfer capacity [10], and Fe–C interactions are central to the redox behavior of iron-modified biochar [5]. At the pore–mineral interface, iron loading must be balanced against porosity: ball milling develops porosity and surface acid functional groups [40], whereas excess iron can block pores or, as discussed in Section 4.3, even suppress uptake [41].

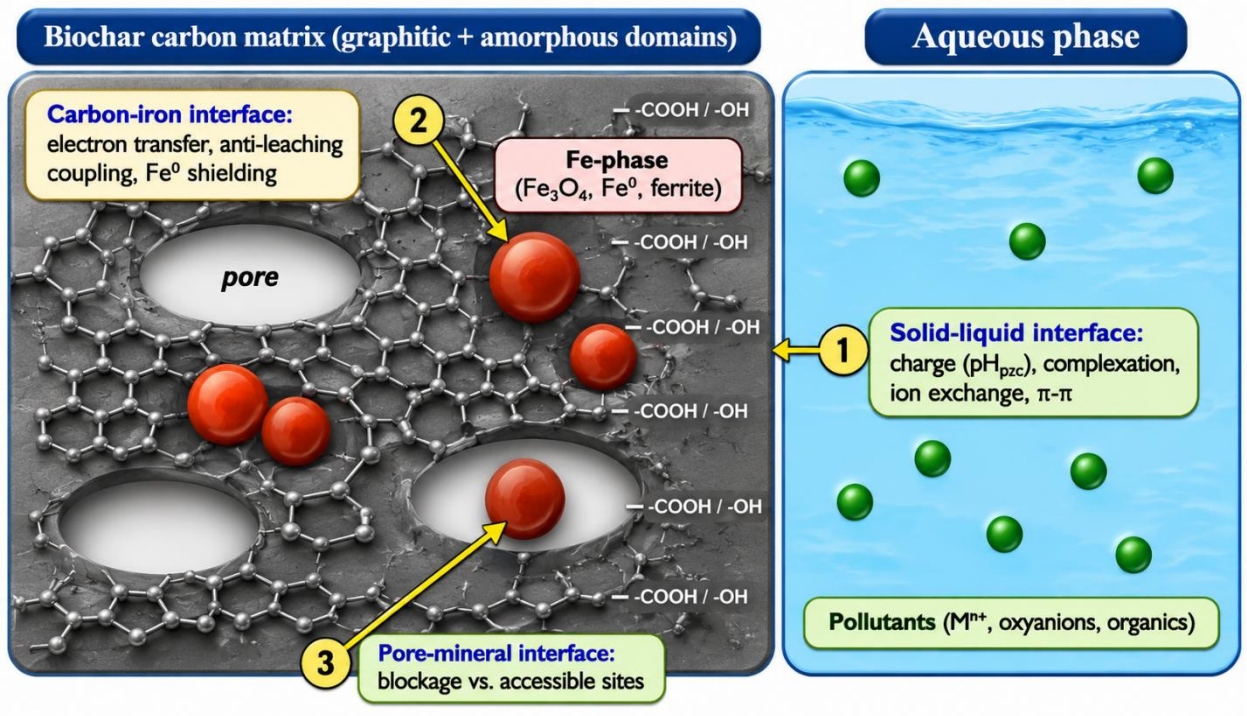

Figure 1. *Schematic of the three interfaces that control magnetic biochar performance: (1) solid–liquid, (2) carbon–iron and (3) pore–mineral. Conceptual illustration synthesized from refs [5, 10, 39–41].*

3. Green Activation and Magnetization Strategies

3.1 Design logic: where iron enters and how the carbon is activated

Magnetic biochar can be categorized by when iron is introduced (pre-pyrolysis impregnation, post-pyrolysis co-precipitation, or simultaneous in situ formation) and how the carbon is activated [1, 3, 5]. Magnetic biochar for antibiotic removal can be made by thermochemistry, co-precipitation or ball milling [4]. Two-step and one-pot syntheses are the most widely used [42]. A recurring trade-off is that magnetic nanoparticles can occupy adsorption sites, so that gains in separability may come at the cost of capacity [18]. Green modifications therefore aim to build porosity and functional groups with the mildest effective activator, and to introduce iron in a form that is well dispersed, strongly coupled to carbon and free of hazardous reductants.

Figure 2 maps the iron-introduction and activation pathways discussed in the following subsections.

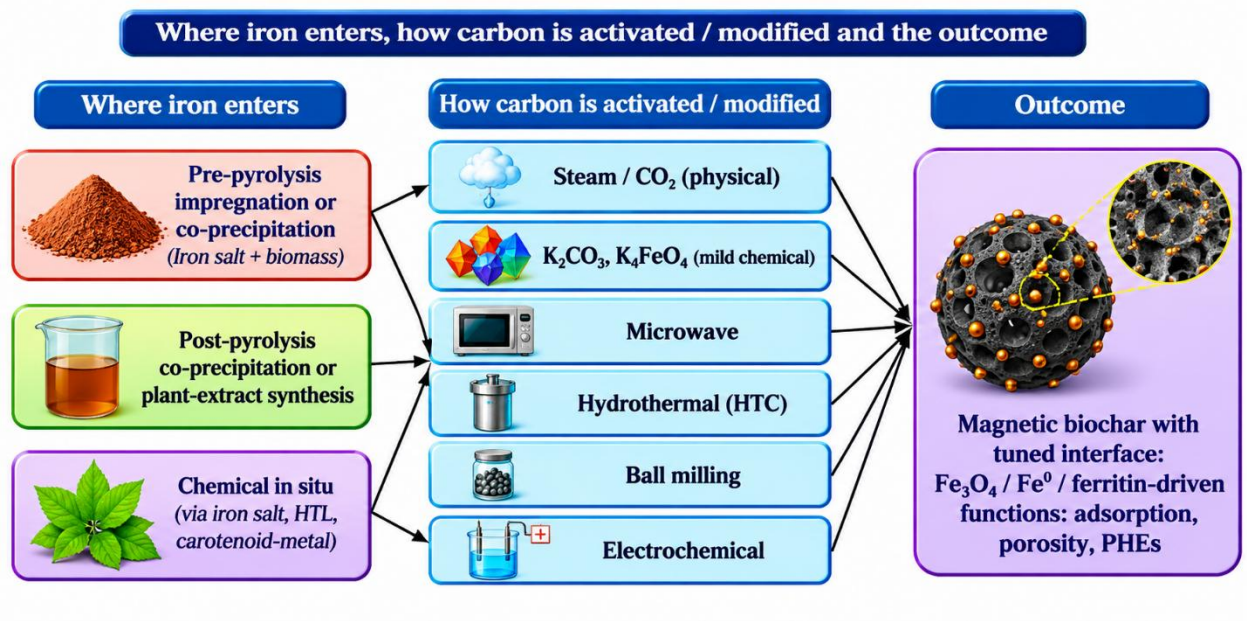

Figure 2. *Iron-introduction pathways and green activation or modification steps for magnetic biochar. Examples: impregnation–coprecipitation on tea-residue biochar [27]; green synthesis on biochar [13]; sludge-based one-pot synthesis [42]; K_2CO_3 and K_2FeO_4 routes [16, 17, 18]; microwave [53, 54]; hydrothermal [57, 59]; ball milling [60, 61]; electrochemical modification [62].*

3.2 Physical activation with steam and CO_2

Steam and CO_2 activation develop porosity by controlled gasification of carbon without liquid activating agents, and are grouped with the physical modifications (steam activation, heat treatment, ball milling) that increase porosity and surface area [5]. Reviews of biomass-based activated carbon discuss physical and chemical activation as the two principal families of routes, with the activating-agent ratio, temperature and duration controlling surface area and porosity [43]. Higher pyrolysis temperature likewise raises porosity and specific surface area of modified biochars for antibiotic adsorption [30]. For magnetic biochar the main design issue is that an oxidizing gas can also oxidize reduced iron, so temperature and exposure must be tuned to retain the intended iron phase [5, 32]. Physical routes are scalable and produce little chemical waste, but are energy intensive and generally build fewer surface functional groups than chemical routes.

3.3 Milder and oxidant-assisted chemical activation

Where chemical activation is needed, alternatives to concentrated KOH, $ZnCl_2$ or H_3PO_4 are attractive. Potassium carbonate is considerably more benign than KOH and has been used to activate and magnetize rice straw in a single step, giving a K_2CO_3-modified magnetic biochar for tetracycline removal [18]. A magnetic K_2CO_3-activated carbon from bamboo shoot was evaluated for rhodamine B adsorption and CO_2 capture [44], and K_2CO_3 activation assisted by ball milling produced a biochar with a BET surface area of 1638 $m^2\ g^{-1}$ and a pore volume of 1.07 $cm^3\ g^{-1}$ for norfloxacin removal [45]. A magnetic eucalyptus carbon was prepared by pretreating biochar with $FeCl_3$ and then activating it with K_2CO_3; its Cr(VI) removal involved adsorption, electrostatic attraction, pore filling, complexation and ion exchange [46]. Where KOH is retained, its use can be optimized: KOH-activated, $FeCl_3$-magnetized coconut-shell biochar was prepared with the KOH amount and $FeCl_3$ concentration tuned to cut pollution and cost [47], and KOH-modified rubber-wood biochar removed 1.85 times more tetracycline and 6 times more Cr(VI) than the unmodified material [48].

A second strategy uses the iron reagent itself as the oxidant. Potassium ferrate (K_2FeO_4) acts as both iron source and activator: oxidative pyrolysis of bamboo shoot shell with K_2FeO_4 gave an activated carbon of ultrahigh surface area with a methylene blue capacity of 560.94 mg g^{-1} [49], and oxidative hydrothermal carbonization of rice straw with K_2FeO_4 yielded a magnetic biochar with enhanced graphitization and oxygen functionality that degraded 99.74% of 75 mg L^{-1} phenol in a Fenton-like system [16]. Hydrothermal growth of Mg–Fe layered double hydroxides on magnetic biochar combines porosity with anion-exchange functionality [37]. Organic acids and mild oxidants can introduce carboxyl groups and act as chelators during iron loading, although studies in the 2021–2026 window that isolate this effect on magnetic biochar remain scarce.

3.4 Plant-extract and biogenic iron synthesis

Plant extracts supply polyphenols and antioxidants that reduce and stabilize iron nanoparticles, replacing hazardous reductants. A leaf-extract route produced Fe_3O_4 nanoparticles that adsorbed methylene blue and could be recycled with a magnet [50]. On biochar, white-tea residue was used to introduce green-synthesized magnetic nanoparticles of about 20–50 nm distributed on the surface, whereas conventional co-precipitation gave serious aggregation; the co-precipitated Fe_3O_4 was purer, while the green product contained small amounts of other iron compounds [13].

The same system showed higher Cr(VI) adsorption capacity and saturation magnetization than the plain biochar [12]. Guava-leaf-extract magnetite on water-lettuce biochar has also been used to activate periodate [51]. Reduced iron is difficult to stabilize in extract-based synthesis because of its susceptibility to oxidation [32], and reproducibility depends on extract composition, so extract characterization should be reported [32, 50].

3.5 Waste-derived and recycled iron sources

Using wastes as iron sources reduces reagent burden. Fenton sludge with sewage sludge gave Fe_3O_4-doped biochar for persulfate activation [14]; pharmaceutical sludge provided endogenous iron for Fe_xN formation [15]; and red mud, an iron-rich alumina by-product, produced biochar with uniformly dispersed Fe_3O_4 [28]. In a solvent-free route, sewage-sludge-derived magnetic biochar with 2% Fe gave the highest capacity, increasing from 113.64 to 151.52 mg g^{-1} for Pb^{2+}, from 101.01 to 109.89 mg g^{-1} for Cd^{2+} and from 57.80 to 74.07 mg g^{-1} for Cu^{2+} as temperature rose from 25 to 45 °C [42]. Expired iron-rich pharmaceutical supplements were converted by hydrothermal carbonization into hydrochar embedding magnetite and maghemite nanoparticles, with life-cycle assessment indicating lower impacts than co-precipitation and pyrolysis/gasification [25]. Exhausted magnetic biochar carrying adsorbed Cu^{2+} has itself been recycled as a PMS activator for norfloxacin degradation [52], illustrating circular reuse of spent sorbent. Heterogeneity and possible trace metals require leachate screening before deployment.

3.6 Microwave-assisted processing

Microwave heating offers rapid, volumetric heating and is among the preparation methods compared in recent reviews [1, 19]. Magnetic porous biochar with a high specific surface area was prepared from water hyacinth by microwave-assisted hydrothermal and pyrolysis treatments for Cr(VI) and tetracycline adsorption [53]. A one-step microwave-assisted synthesis of MgO-modified magnetic biochar was reported for combined lead and phosphate removal [54], and microwave-assisted hydrothermal preparation gave hydrochar-supported iron nanoparticles that removed organophosphorus insecticides with Langmuir capacities of about 3.1–3.2 mg g^{-1} by endothermic chemisorption [55]. Microwave modification of a calcium-rich biochar with β-cyclodextrin raised tetracycline capacity from 142.36 mg g^{-1} at 25 °C to 161.91 mg g^{-1} at 45 °C [56]. Non-uniform temperature fields and scale-up of microwave cavities remain practical challenges.

3.7 Hydrothermal and solvothermal routes

Hydrothermal routes operate at moderate temperatures in water and are attracting growing interest for magnetic biochar [3]. A one-step hydrothermal conversion of black liquor with 1 M Fe^{3+} gave a magnetic hydrochar with a surface area of 171.4 $m^2\ g^{-1}$, a pore volume of 0.146 $cm^3\ g^{-1}$, a saturation magnetization of 33.7 emu g^{-1} and a methylene blue capacity of 97.40 mg g^{-1}, retaining 83.19% after five cycles [57]. Optimization of residence temperature (180–220 °C) and time (6–24 h) identified 220 °C and 12 h as the best conditions for one-step carbonization and magnetization of pomegranate waste [58]. Iron-doped hydrochars from flax shives and eucalyptus sawdust raised surface area from below 5 $m^2\ g^{-1}$ to 87–118 $m^2\ g^{-1}$, removed 95% and 88% of pentachlorophenol, and showed no iron leaching over six cycles [59]. Hydrothermal growth of Mg–Fe LDH [37] and hydrothermal carbonization of pharmaceutical waste [25] are further examples. Process-water treatment and lower surface area than pyrolytic chars are the usual drawbacks.

3.8 Mechanochemical (ball-milling) modification

Ball milling is a largely solvent-free route that reduces particle size, develops porosity and acid functional groups [40] and enables incorporation of nanoparticles; reviews cover ball-milling synthesis of biochar nanocomposites for emerging contaminants [11]. Ball milling cotton-husk biochar with γ-Fe_2O_3 followed by reductive calcination gave a nano-ZVI-supporting magnetic biochar with capacities of 266.7 mg g^{-1} for oxytetracycline and 83.36 mg g^{-1} for ciprofloxacin (1.6 and 2.3 times those of the unmilled biochar), ethanol-plus-ultrasound regeneration, and low iron leaching between pH 3 and 11 [60]. Fe_3O_4 on ball-milled biochar activated persulfate for bisphenol A removal, with oxygen groups, graphitization, mesopores and Fe^{3+}/Fe^{2+} conversion facilitating activation [61], and ball-milled sulfur-doped nano-ZVI on biochar has been used for phosphorus removal [33]. Energy use and contamination from milling media should be evaluated.

3.9 Low-temperature carbothermal and one-pot routes

Carbothermal reduction normally requires 800 °C or more to convert iron oxides to Fe^0, which is energy intensive. A K_2FeO_4/NaOH route lowered this to 300–500 °C, with effective reduction at 400 °C; the ZVI-doped biochar reached a saturation magnetization of 56.3 emu g^{-1} and capacities of 1106.25 mg g^{-1} for tetracycline and 182.03 mg g^{-1} for ciprofloxacin [17]. The formation mechanism of graphene-encapsulated Fe^0 on biochar has been investigated over 600–1000 °C,

for four iron sources and iron loadings of 5–40% [38], and sludge-based one-pot syntheses omit separate magnetization steps [42]. These routes show how energy demand can be cut while retaining a strongly magnetic phase.

3.10 Electrochemical and other surface modification

Electrochemical modification can tune surface chemistry in a reagent-light manner; a one-step and an electrochemical method for modifying magnetic biochar were compared for their effect on phosphate adsorption [62]. Plasma treatments are conceptually similar but are far less reported for magnetic biochar in the 2021–2026 literature, so their potential remains largely unquantified.

3.11 Comparative overview

Table 2 summarizes the routes, Figure 3 gives a qualitative, literature-informed comparison, and Table 3 and Figure 4 collect reported quantitative outcomes. The scores in Figure 3 are our own qualitative judgments derived from the evidence cited in Table 2, not measured values.

Table 2. *Green activation and magnetization routes for magnetic biochar and their interfacial consequences.*

Route	Principle	Interface effect	Example evidence	Limitation	Ref.
Steam / CO_2 activation	Gasification of carbon	Porosity development	Physical modification raises porosity and surface area	Oxidation of Fe phases; energy	[5, 30, 43]
Mild chemical (K_2CO_3, LDH growth)	Less corrosive activation	Micro/mesoporosity; anion-exchange sites	K_2CO_3-magnetic biochar; 1638 $m^2\ g^{-1}$ with ball milling	Residual alkali; wash water	[18, 37, 45, 46]
Oxidant-assisted (K_2FeO_4)	Iron salt as activator	Graphitization, O-groups, ZVI	99.74% phenol degradation; 560.94 mg g^{-1} MB	Reagent cost; waste liquor	[16, 17, 49]
Plant-extract Fe synthesis	Polyphenol reduction and	Dispersed 20–50 nm particles	White-tea magnetic	Batch variability;	[12, 13,

	capping		biochar; leaf-extract Fe_3O_4	mixed iron phases	50, 51]
Waste-derived / recycled Fe	Carbothermal formation from by-products	Fe_3O_4, Fe_xN formation	Fenton sludge, pharmaceutical sludge, red mud	Heterogeneity; trace metals	[14, 15, 25, 28, 42, 52]
Microwave	Volumetric heating	Rapid pore and phase formation	MgO magnetic biochar; water-hyacinth MBC	Hot spots; scale-up	[53–56]
Hydrothermal	Subcritical water	O-group-rich surfaces	Black-liquor hydrochar; flax-shive hydrochar	Process water; lower porosity	[3, 25, 37, 57, 59]
Ball milling	Mechanochemical	Porosity, acid groups, Fe–C contact	Milled cotton-husk MBC; Fe_3O_4 on milled biochar	Energy; media contamination	[11, 33, 40, 60, 61]
Low-T carbothermal	Reductant-assisted reduction	Fe^0 at 400 °C	Ms 56.3 emu g^{-1}	Narrow evidence base	[17, 38]
Electrochemical	Surface redox	Surface chemistry tuning	Electrochemically modified MBC	Maturity	[62]

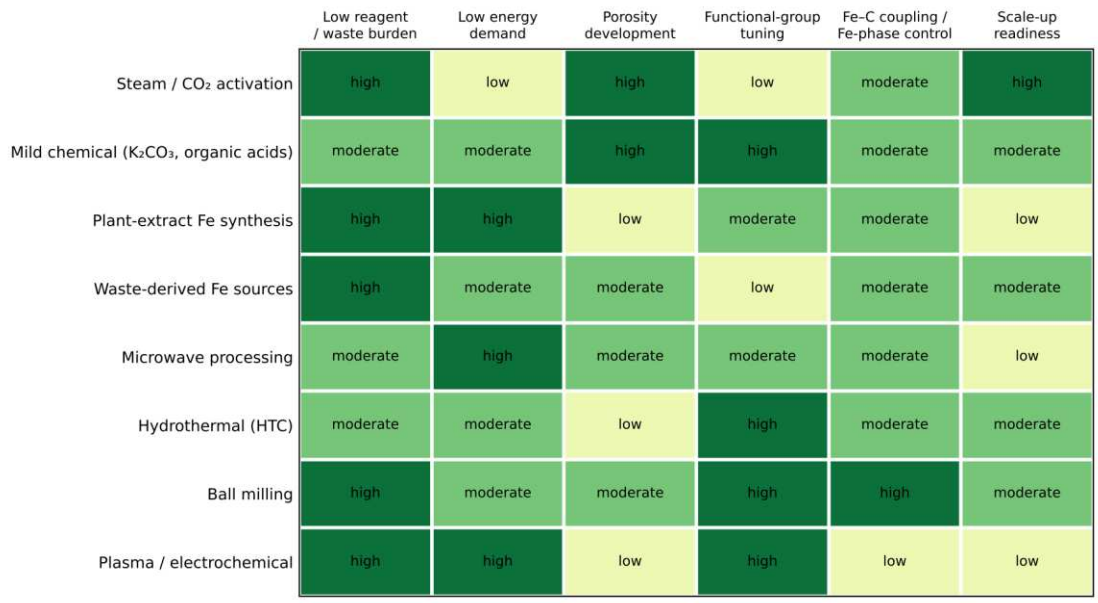

Figure 3. *Qualitative comparison of green activation routes against six criteria (low reagent burden, low energy demand, porosity development, functional-group tuning, Fe–C coupling and Fe-phase control, scale-up readiness). Scores are the authors' qualitative synthesis of refs [3, 5, 11, 13, 16–18, 25, 30, 33, 37, 38, 40, 43–64].*

Table 3. *Reported properties and performance of materials prepared by green or reduced-impact routes.*

Route and material	Preparation condition	Reported property	Reported performance	Ref.
K_2FeO_4/NaOH carbothermal, ZVI-doped biochar	400 °C	Ms 56.3 emu g^{-1}	TC 1106.25; CIP 182.03 mg g^{-1}	[17]
Ball-milled γ-Fe_2O_3 cotton-husk biochar	Reductive calcination	Low Fe leaching, pH 3–11	OTC 266.7; CIP 83.36 mg g^{-1}	[60]
One-step hydrothermal black-liquor hydrochar	1 M Fe^{3+}	171.4 m^2 g^{-1}; Ms 33.7 emu g^{-1}	MB 97.40 mg g^{-1}; 83.19% after 5 cycles	[57]
Mg–Fe LDH on magnetic biochar	Hydrothermal	Ms 2.63 emu g^{-1}	Phosphate recovery	[37]
Sludge-derived magnetic biochar	2% Fe, solvent-free	Optimal Fe content	Pb 151.52; Cd 109.89; Cu 74.07 mg g^{-1} (45	[42]

			°C)	
Flax-shive / eucalyptus iron-doped hydrochar	HTC with Fe	87–118 m^2 g^{-1} (from <5)	PCP 95% / 88%; six cycles, no Fe leaching	[59]
K_2CO_3 + ball milling biochar (non-magnetic)	K_2CO_3 activation	1638 m^2 g^{-1}; 1.07 cm^3 g^{-1}	Norfloxacin removal	[45]
KOH-modified rubber-wood biochar (non-magnetic)	KOH	Improved pores and redox capacity	TC ×1.85; Cr(VI) ×6 vs unmodified	[48]

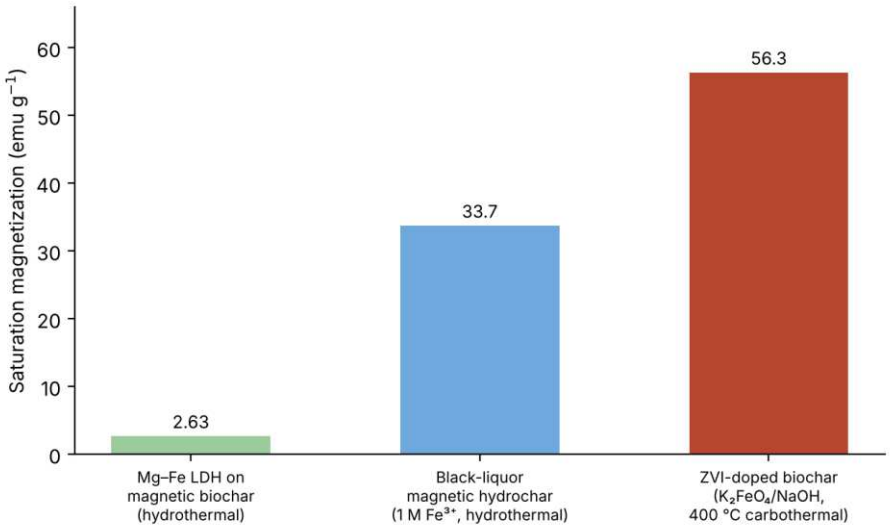

Figure 4. *Saturation magnetization reported for three green-prepared magnetic carbons spanning more than one order of magnitude. Data from refs [17, 37, 57].*

4. Linking Processing to Surface Functionality

4.1 Characterizing the surface: what each probe can and cannot show

Interfacial claims are only as good as the measurements behind them. Biochars contain far fewer functional groups than their biomass precursors, so FTIR bands are often broad and overlapping; X-ray photoelectron spectroscopy probes only about the outer 10 nm; and Boehm titration separates strongly, mildly and weakly acidic groups that are assigned to carboxyl, lactonic and phenolic functions [65]. Surface charge is complementary, derived from the point of zero charge and zeta potential. For magnetic biochar the iron phase must be identified by diffraction and magnetometry and, ideally, by Mössbauer spectroscopy, since phases such as magnetite and maghemite are easily confused [5]. Physico-chemical characterization of magnetized walnut-

shell biochars illustrates a minimum set: elemental and ash analysis, FTIR, BET, zeta potential, pH_{pzc} and saturation magnetization [29].

4.2 Functional groups and heteroatoms

Carboxyl, hydroxyl, amino and sulfur-containing groups differ in their affinity and mechanism towards individual contaminants. In the bifunctionalized magnetic biochar, grafting cystamine (ligand) and glutaraldehyde (crosslinker) onto alkali-treated magnetic biochar raised Cr(VI) removal through reduction by amino, sulfur and Fe(II) sites combined with electrostatic attraction [39]. In sulfonamide sorption, hydrogen bonding and π-bond-assisted hydrogen bonding determined affinity, and oxygen-containing groups rather than the iron mineral phase dominated hydrogen-bond energy [66]. Likewise, hydrogen bonding, π–π, electrostatic and hydrophobic interactions and intrapore diffusion contributed to tetracycline uptake by peanut-shell magnetic biochar, which removed more than 85% over a wide pH range [67]. Amino functionalization with APTES gave a pine-needle magnetic biochar that removed up to 97% of Pb(II) and Cd(II) at basic pH, with the $–NH_2$ signal decreasing after uptake [68]. The iron-anchoring chemistry itself matters: FeO, $FeSO_4$ and $FeCl_3$ were compared as iron sources for anchoring and for Remazol Brilliant Blue R uptake, with a Langmuir maximum capacity of 11.33 mg g^{-1} [69]. Reviews of modified biochar for arsenic, cadmium and chromium removal connect the choice of modification to the dominant binding mechanism [70–72]. Nitrogen doping with iron has also been exploited: kelp-derived self-nitrogen-doped biochar stabilized Fe nanoparticles for PMS activation [73], N-doped magnetic biochar has been applied to sulfonamides [74], and Fe_xN formation from exogenous nitrogen enhanced oxidant activation [15].

4.3 Porosity, iron loading and accessibility

Magnetization tends to trade surface area for recoverability, so there is usually an optimal iron loading. In sludge-derived magnetic biochar, Pb^{2+}, Cd^{2+} and Cu^{2+} capacities peaked at 2% Fe [42], and for chlorinated aliphatic hydrocarbons a 10% Fe_3O_4 loading was best, with adsorption improved by 34.40–222.25% over pyrolysis at 500–900 °C [63]. The effect can also be negative: magnetite activation reduced Pb(II) adsorption by up to 86% across four feedstocks and three pyrolysis temperatures, apparently because it decreased ash content, pH and exchangeable cations, and the authors concluded that feedstock type and pyrolysis temperature mattered more than Fe_3O_4 activation [41]. Conversely, iron doping of hydrochars raised surface area from below

5 to 87–118 $m^2\ g^{-1}$ [59], and ball milling develops porosity and surface acid groups [40, 61]. Activation before iron loading and the use of dispersing agents help preserve accessible sites [5, 13], and Fe-doped adsorbents that retain porosity can combine capacity with magnetic separation [18, 75].

Figure 5 compares reported surface areas, and Figure 6 collects the reported changes on iron incorporation.

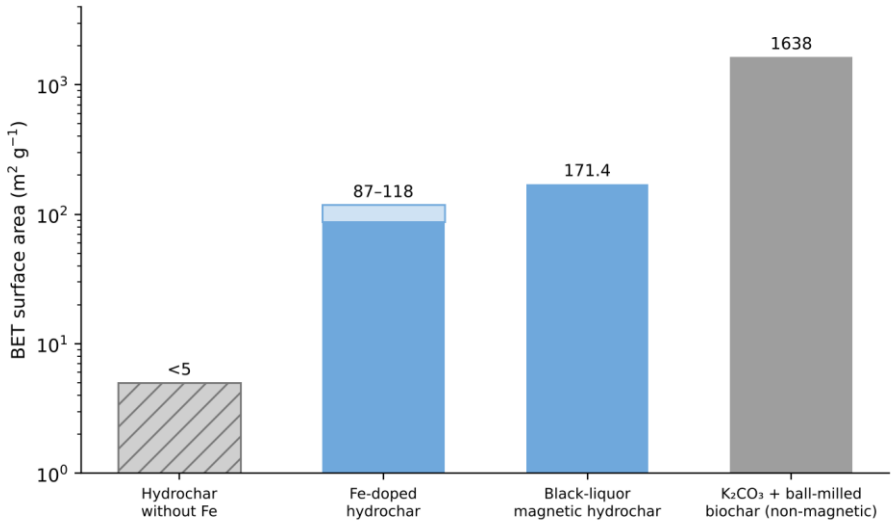

Figure 5. *Reported BET surface areas: hydrochars without and with iron doping [59], black-liquor magnetic hydrochar [57] and a K_2CO_3-activated, ball-milled biochar (non-magnetic) [45]. Logarithmic axis.*

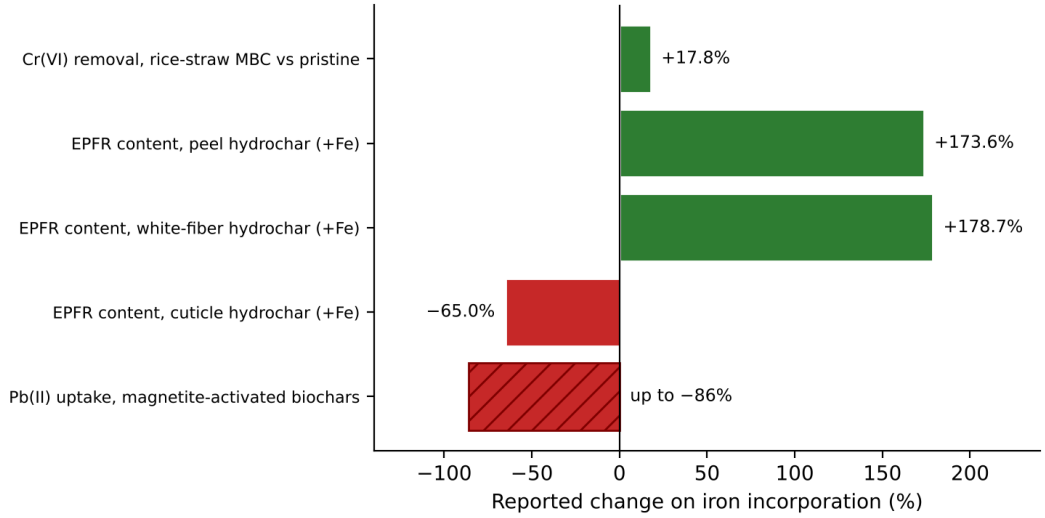

Figure 6. *Percentage change reported on iron incorporation: Cr(VI) removal by magnetic versus pristine biochar [39], EPFR content of three pomelo-derived hydrochars [78] and the maximum loss of Pb(II) uptake after magnetite activation [41]. Cr(VI) and EPFR values are calculated from the reported data.*

4.4 Iron speciation, dispersion and carbon–iron coupling

Iron speciation depends on precursor, atmosphere, temperature and reductant availability. Iron–carbon interactions determine adsorption, redox activity and electron transfer, and iron leaching, regeneration and environmental risk remain open [5]. Temperature and reagent choice shift the dominant phase: a K_2FeO_4/NaOH system produced Fe^0 at 400 °C [17], whereas graphene-encapsulated Fe^0 formed over 600–1000 °C depending on iron source and loading [38]. Metal modification also limits leaching of metal ions and raises conductivity, which helps oxidant activation [30]. Strong interaction between Fe^{2+}/Fe^{3+} and graphitized biochar improved the cycling stability of a kelp-derived Fe/biochar PMS activator [73], graphitization was highlighted for Co/N co-doped magnetic biochar [76], and Fe-doped hydrochars retained their iron phases after reuse without detectable leaching [59]. Green-synthesized particles were smaller and better dispersed than co-precipitated ones but contained mixed iron phases [13], illustrating the trade-off between dispersion and phase purity.

4.5 Persistent free radicals and redox-active carbon sites

Persistent free radicals (PFRs) are formed during pyrolysis and mediate both direct pollutant transformation and oxidant activation, although they also carry ecological risks that call for management during production and application [8]. Reviews of their catalytic capability

highlight roles in advanced oxidation, Cr(VI) reduction and As(III) oxidation, with formation mechanisms and detection methods [9]. A systematic review reports that •OH is associated with surface –OH and oxygen-centered PFRs, whereas $O_2^{\bullet -}$ is linked to quinone structures and carbon-centered radicals [7]. Iron interacts with these sites in both directions. Biochar accelerated the sluggish Fe^{3+}/Fe^{2+} cycle in a Fe^{3+}/persulfate system: medium-temperature biochar (BC500) enhanced the first-order rate constant by 5.2- and 35.7-fold relative to the low- and high-temperature chars, with PFRs, phenolic –OH and edge defects mediating electron transfer, and the non-radical Fe(IV) contribution reaching 56.3% [77]. In pomelo-peel hydrochars, iron doping raised EPFR content from 3.33 to 9.11 × 10^{18} spins g^{-1} (peel) and from 2.96 to 8.25 × 10^{18} spins g^{-1} (white fiber), but excess iron in the cuticle-derived hydrochar lowered it from 7.95 to 2.78 × 10^{18} spins g^{-1}, presumably by consuming the radicals (Figure 7) [78]. Oxidative hydrothermal carbonization introduced multiple iron species together with PFRs, giving diverse catalytic sites that facilitated Fe^{3+}/Fe^{2+} cycling [16]. Interface design must therefore treat iron loading as a variable with an optimum, not a monotonic benefit.

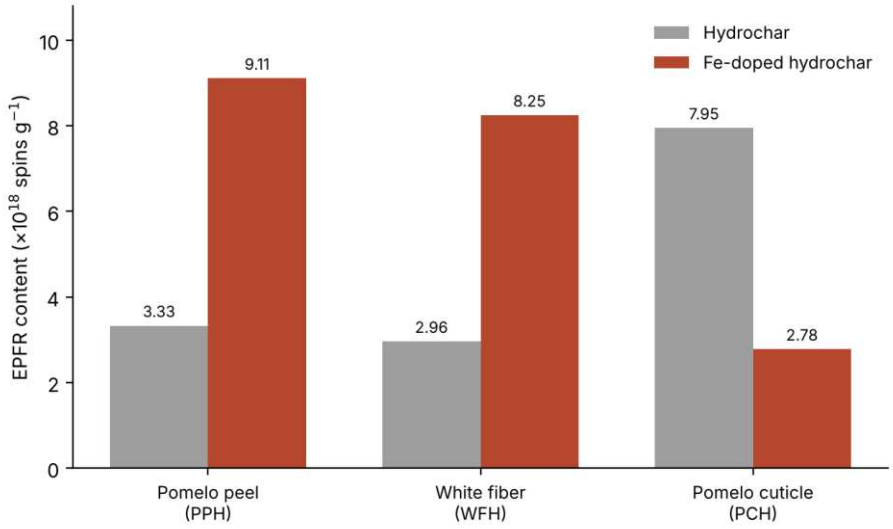

Figure 7. *Environmental persistent free radical (EPFR) content of pomelo-peel-derived hydrochars with and without iron doping, showing that iron can raise or lower EPFR content depending on the precursor. Data from ref [78].*

4.6 Surface charge and pH dependence

Electrostatic attraction between anionic Cr(VI) and positively charged surfaces, together with reduction, controlled Cr(VI) uptake by the bifunctionalized material, whose maximum capacity was 66.10 mg g^{-1} at 50 °C and pH 2, fitting pseudo-second-order and Langmuir models;

coexisting Cl^-, NO_3^-, SO_4^{2-} and HPO_4^{2-} reduced removal by 7.58% [39]. Basic pH favored Pb(II) and Cd(II) removal by APTES-functionalized magnetic biochar [68]. The pH dependence of oxyanion removal is a general feature of magnetic biochars [46, 79], and zeta potential and pH_{pzc} values should accompany any pH-edge data [29].

4.7 Synthesis of structure–function relationships

Table 4 condenses the processing–structure–function links discussed above.

Table 4. *Structure–processing–function relationships in magnetic biochar interfaces.*

Structural feature	Processing handle	Documented effect	Ref.
Oxygen-containing groups	Mild oxidation; oxidative K_2FeO_4 route; HTC	Dominate H-bond energy with sulfonamides; support Fenton-like activity	[16, 66]
Amino / sulfur ligands	Cystamine, APTES grafting	Cr(VI) reduction and electrostatic attraction; 97% Pb/Cd removal at basic pH	[39, 68]
Iron loading	Fe/C ratio; Fe salt concentration	Optimum at 2–10% Fe in different systems; up to 86% loss of Pb uptake with magnetite activation	[41, 42, 63]
Iron phase (Fe_3O_4 vs Fe^0)	Temperature; reductant; iron source	Fe^0 at 400 °C with K_2FeO_4/NaOH; Ms 56.3 emu g^{-1}	[17, 38]
Graphitization / carbon coupling	Pyrolysis temperature; N or Co doping	Stable Fe cycling; improved PMS activation	[73, 76]
PFRs / defects	Pyrolysis temperature; Fe doping	BC500 optimum; EPFR content rises or falls with iron	[77, 78]
Surface area / pore volume	Activation; ball milling; HTC	1638 m^2 g^{-1} (K_2CO_3 + milling); <5 to 87–118 m^2 g^{-1} (HTC with Fe)	[45, 59]
Surface charge	pH; functionalization	Electrostatic control of oxyanions and cations	[39, 68]

5. Interfacial Mechanisms of Pollutant Removal

Removal is rarely governed by one mechanism (Table 5). For Cr(VI), adsorption, electrostatic attraction, pore filling, complexation and ion exchange have all been invoked [46], and reduction of Cr(VI) to Cr(III) by Fe(II) and by functional groups followed by binding of Cr(III) is

frequently decisive [39, 79]. Because Cr(III) may be released again with increasing contact time, coupled reduction and adsorption is necessary [39]. For Pb^{2+}, Cd^{2+} and Cu^{2+} on sludge-derived magnetic biochar, surface complexation, cation–π interaction, ion exchange and electrostatic attraction were involved [42], and for Cd on MgO- and Fe_3O_4-loaded biochar, precipitation and ion exchange accounted for the passivation mechanism [80]. For arsenic, magnetic biochars have been tested in aqueous solution, groundwater and contaminated paddy soil [81], and reviews summarize how modification enhances arsenic removal [70, 72]. In the corolla-like MnO_2-decorated magnetic biochar, Fe_3O_4, MnO_2 and biochar all contributed to As(V) and Cr(VI) uptake, Cr(VI) was selectively reduced by Fe_3O_4, and competitive adsorption was probed with density functional theory [79]. For antibiotics, site-energy-distribution analysis of competitive sulfamethoxazole and bisphenol A adsorption on magnetic biochar [82] and the sulfonamide mechanism study [66] point to hydrogen bonding and π-interactions as the main binding modes, and combined adsorption of several organic contaminants on magnetic biochar has also been examined [64].

Figure 8 illustrates the principal surface mechanisms listed in Table 5.

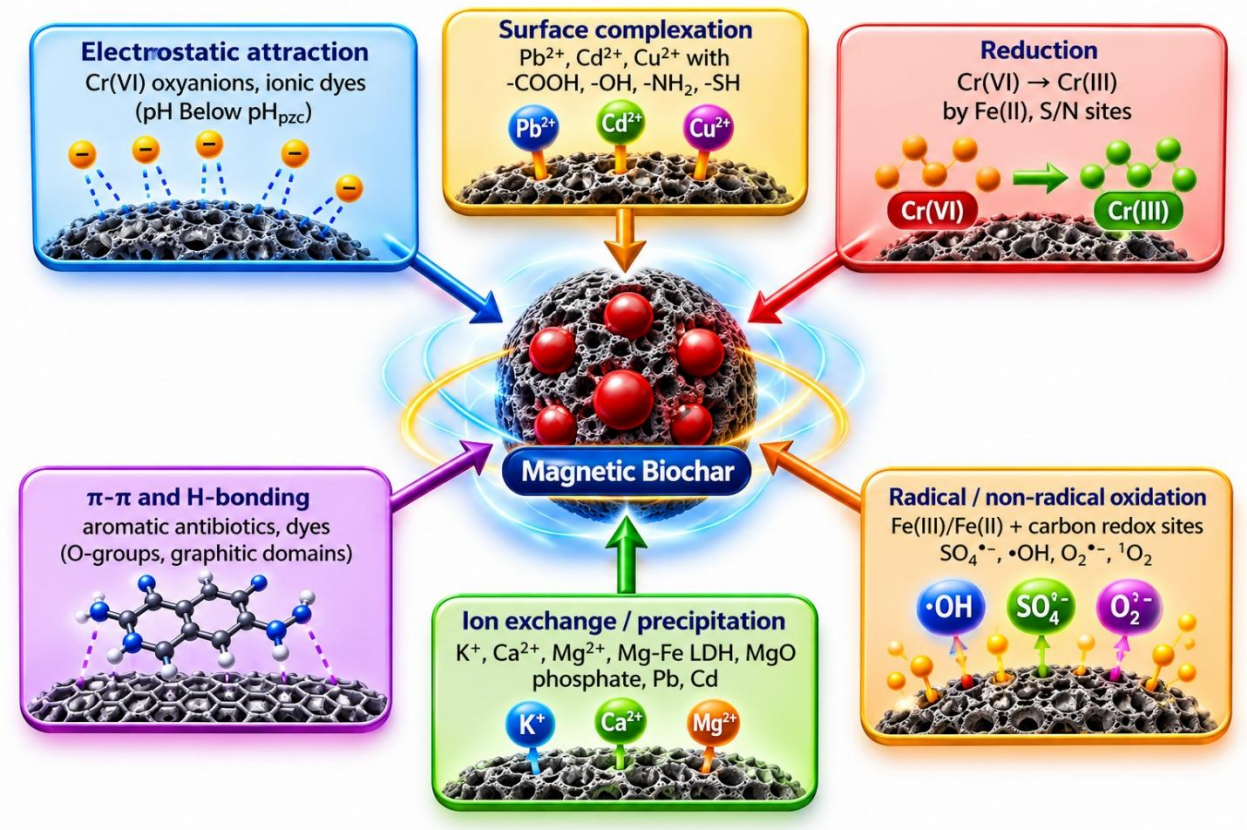

Figure 8. *Principal interfacial mechanisms at magnetic biochar surfaces and the contaminants they address. Synthesized from refs [27, 34, 39, 42, 66, 79, 80].*

Table 5. *Interfacial sites, targets and dominant mechanisms in magnetic biochar systems.*

Site / feature	Typical target	Dominant mechanism	Evidence	Ref.
Carboxyl, hydroxyl, amino, S-groups	Cr(VI), metal cations	Complexation, electrostatic attraction, reduction	Bifunctionalized MBC; eucalyptus MBC	[39, 42, 46]
Fe_3O_4 / Fe(II)	Cr(VI), As(V)	Redox reduction followed by binding of Cr(III)	Corolla-like MnO_2/Fe_3O_4 biochar with DFT	[79]
Mg-based phases (LDH, MgO)	Phosphate, Pb, Cd	Anion exchange, precipitation	Mg–Fe LDH; MgO MBC; BC-Mg	[37, 54, 80]
Graphitic	Aromatic	π–π, hydrogen	Sulfonamides;	[66,

domains, O-groups	organics, antibiotics	bonding	tetracyclines	67, 82]
Fe(II)/Fe(III) + carbon redox sites	Antibiotics, bisphenol A	Radical and non-radical oxidation	PMS/persulfate systems (Table 7)	[7, 27, 34, 61]
Pores / mesopores	Organics, oxidant access	Pore filling, mass transfer	Ball-milled biochar	[40, 60, 61]

For oxidation, magnetic biochars activate PMS or persulfate to generate sulfate and hydroxyl radicals and superoxide, together with non-radical pathways such as singlet oxygen and electron transfer (Figure 9). Quenching and electron paramagnetic resonance (EPR) analyses are the standard evidence [27, 61]. The balance depends on the material: $O_2^{\bullet -}$ was dominant in $MnFe_2O_4$@BC, followed by singlet oxygen [34]; a non-radical pathway dominated in kelp-derived Fe@BC [73]; radicals contributed about 56% versus about 44% non-radical in a red-mud biochar [28]; and oxygen-centered radicals of hydrochar were decisive in a Fenton-like system for bisphenol A [78]. Because scavenger and EPR evidence can be ambiguous, mechanistic claims should be cross-checked with probe compounds and kinetics.

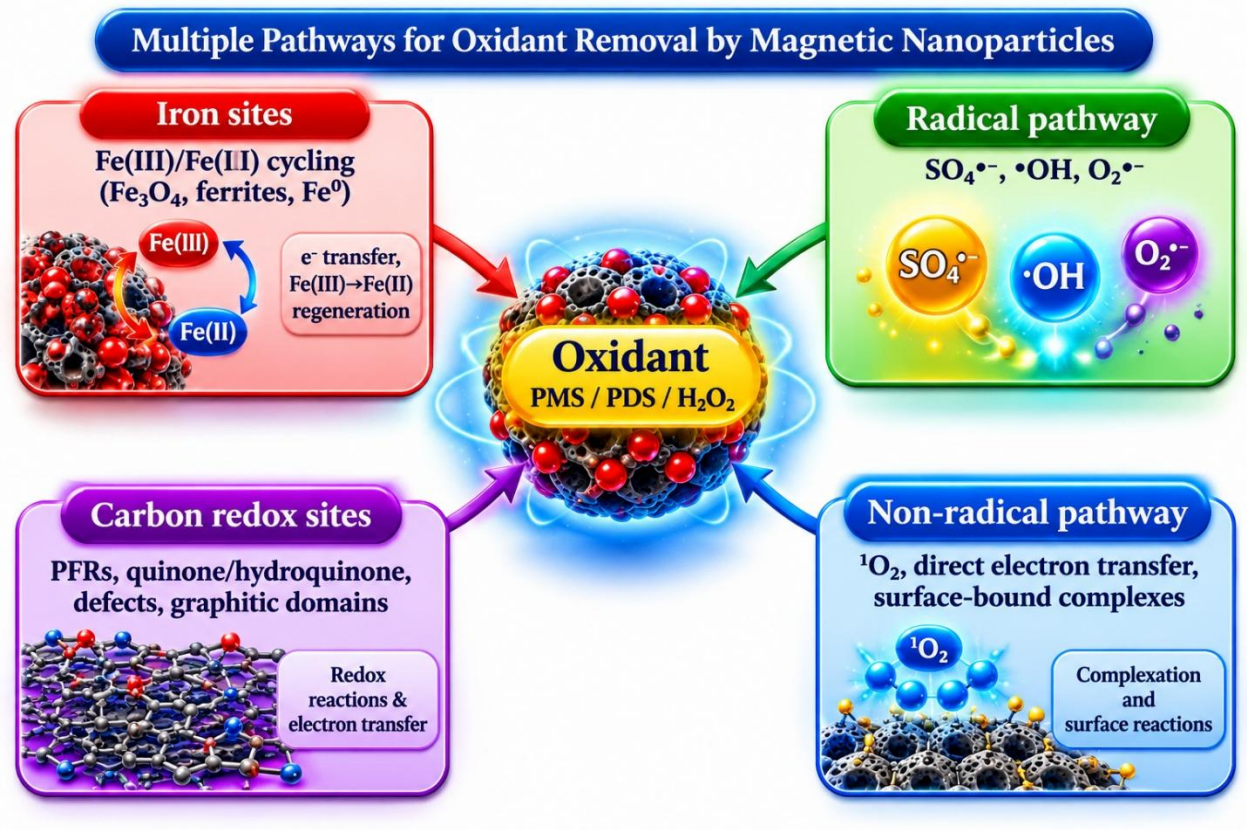

Figure 9. *Mechanistic framework for oxidant activation by magnetic biochar, combining Fe(II)/Fe(III) cycling and carbon redox sites to drive radical and non-radical pathways. Conceptual synthesis of refs [7, 27, 28, 34, 61, 73, 77, 78].*

6. Comparative Analysis of Reported Performance (Results)

This section compares published performance by contaminant class. Reported values are taken from the cited studies and are not directly comparable across studies because pH, dose and matrix differ.

6.1 Heavy metals and metalloids

Table 6 lists representative studies. In the clearest like-for-like comparison, within one rice-straw system, Cr(VI) removal was 61.42% for pristine biochar, 72.37% for magnetic biochar and 100% for the bifunctionalized magnetic biochar (Figure 10) [39]. Magnetization alone therefore contributed about 11 percentage points, while ligand functionalization contributed the larger gain. Similar logic applies to green-synthesized materials, where adding iron nanoparticles improved both Cr(VI) capacity and saturation magnetization [12]. Not all iron additions help, however: magnetite activation reduced Pb(II) adsorption by up to 86% in some biochars [41].

Table 6. *Representative magnetic biochar studies for heavy metals and metalloids.*

Material	Target	Reported result	Key mechanism	Ref.
Bifunctionalized magnetic biochar (rice straw)	Cr(VI)	100% removal vs 72.37% (MBC) and 61.42% (PBC); q_{max} 66.10 mg g^{-1} (50 °C, pH 2); 61.12% after five cycles	Reduction, electrostatic attraction	[39]
Magnetic eucalyptus carbon ($FeCl_3$ + K_2CO_3)	Cr(VI)	Efficient removal reported	Adsorption, pore filling, complexation, ion exchange	[46]
Green-synthesized magnetic biochar (white tea)	Cr(VI)	Higher capacity and Ms than plain biochar	Site-energy-distribution analysis	[12, 13]
MnO_2-decorated porous magnetic biochar	As(V), Cr(VI)	Simultaneous removal; DFT-supported	Reduction by Fe_3O_4; competitive adsorption	[79]
Pinecone magnetic biochar	As	Aqueous, groundwater and paddy soil tested	Adsorption and immobilization	[81]
Sludge-derived magnetic biochar (2% Fe)	Pb, Cd, Cu	151.52, 109.89, 74.07 mg g^{-1} at 45 °C	Complexation, cation–π, ion exchange	[42]
APTES-functionalized pine-needle MBC	Pb(II), Cd(II)	Up to 97% removal at basic pH	Amino-group complexation	[68]
MgO- and Fe_3O_4-loaded biochar	Cd (water, soil)	Adsorption and soil passivation; maize growth tested	Precipitation, ion exchange	[80]
Magnetite-impregnated biochar (4 feedstocks)	Pb(II)	Up to 86% lower uptake after Fe_3O_4 activation	Cation exchange, Ca/Mg vs K/Na	[41]

Bentonite-loaded magnetic biochar	Cu^{2+}, tetracycline	Simultaneous removal	Co-precipitated Fe_3O_4; amphoteric surface	[75]
Mg-based magnetic biochar (microwave)	Pb, phosphate	Simultaneous removal	Precipitation, anion exchange	[54]

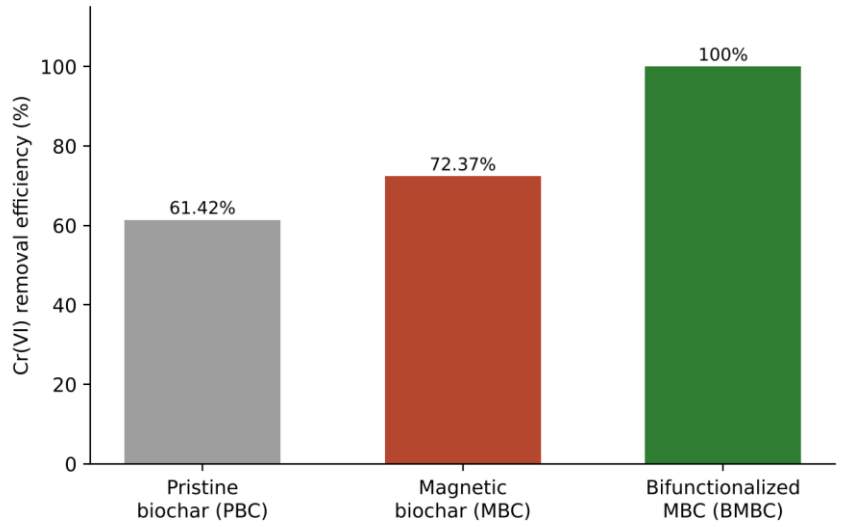

Figure 10. *Cr(VI) removal efficiency of pristine (PBC), magnetic (MBC) and bifunctionalized magnetic biochar (BMBC) from a rice-straw system. Data from ref [39].*

Figure 11 shows the temperature dependence of the capacities reported for sludge-derived magnetic biochar and a calcium-rich biochar.

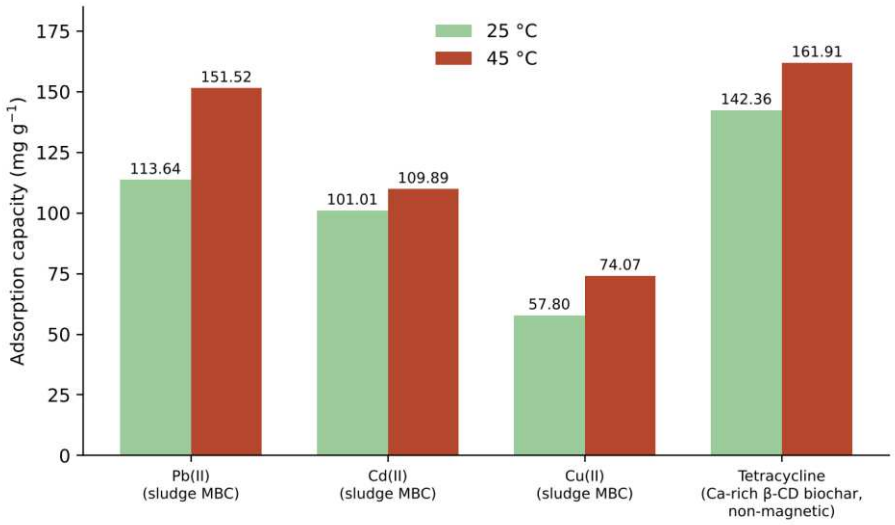

Figure 11. *Adsorption capacities at 25 and 45 °C reported for Pb(II), Cd(II) and Cu(II) on sludge-derived magnetic biochar [42] and for tetracycline on a calcium-rich β-cyclodextrin biochar (non-magnetic comparator) [56].*

6.2 Antibiotics and organic pollutants

For adsorption, antibiotic capacities of magnetic biochar span about 5–900 mg g^{-1} [4], and the highest values reported in this review come from the carbothermal ZVI route (1106.25 mg g^{-1} for tetracycline) [17]. For oxidation, Table 7 compiles magnetic-biochar-activated systems. Across systems, the shared design is an iron or iron-compound phase that cycles between oxidation states on a carbon support that adds redox sites and stabilizes nanoparticles [7, 27, 61]. Metal-modified biochar-assisted oxidation generates more reactive oxygen species and limits metal leaching [30], and reviews of antibiotic removal note that mechanisms are still ambiguous and that secondary pollution and preparation cost are concerns [4]; adsorption of antibiotics and resistance genes by biochar has also been reviewed [83].

Table 7. *Magnetic and iron-modified biochar systems for oxidant activation.*

Catalyst / oxidant	Target	Pathways reported	Notable feature	Ref.
Fe_3O_4@tea-residue biochar / PMS	Tetracycline	Radical quenching and EPR analysis	Pseudo-first-order kinetics	[27]
Fe_3O_4 on ball-milled biochar / persulfate	Bisphenol A	$SO_4^{\bullet-}$, •OH, $O_2^{\bullet-}$ and $^1O_2$	Oxygen groups, mesopores, Fe^{3+}/Fe^{2+}	[61]

			conversion	
$MnFe_2O_4$@BC / PMS	Bisphenol A	Radical and non-radical; $O_2^{\bullet-}$ dominant	Coexisting pathways	[34]
Kelp-derived N-doped Fe@BC / PMS	Tetracycline	Non-radical dominant	Stable recycling via graphitized carbon	[73]
Red-mud biochar / PMS	Tetracycline	~56% radical, ~44% non-radical	RSM optimization; waste valorization	[28]
Fe_3O_4-doped biochar (Fenton + sewage sludge) / persulfate	1-H-1,2,4-triazole	Persulfate activation	Sludge valorization	[14]
Fe_xN pharmaceutical-sludge biochar / PMS	Levofloxacin	Enhanced activation by Fe–N	Endogenous Fe, exogenous N	[15]
Co/N co-doped magnetic biochar / PMS	Tetracycline	Graphitization-assisted	Important role of graphitization	[76]
Cu-doped magnetic biochar / PMS	Sulfamethoxazole	Enhanced by Cu doping	Mechanism of Cu doping	[36]
Fe-doped kelp biochar / PMS	Ciprofloxacin	Multiple active sites, radical and non-radical	Multi-site triggering	[84]
Goethite/biochar / PMS	Tetracycline	Radical and non-radical	Inherent roles of both	[35]
Oxidative-HTC magnetic biochar / H_2O_2	Phenol (75 mg L^{-1})	Fenton-like with PFR participation	99.74% degradation	[16]
Fe-doped pomelo-peel hydrochar / H_2O_2	Bisphenol A	Oxygen-centered radicals, g3-type EPFRs	Long-term reactivity after storage	[78]
Biochar + Fe^{3+} / persulfate	Model organics	Fe(IV) non-radical 56.3%	BC500 optimum; 5.2–35.7× rate gain	[77]

6.3 Adsorption of antibiotics, dyes and nutrients

Table 8 summarizes adsorption systems. Phosphate recovery is a natural fit for magnetic biochar because nutrient-laden material can be recovered and reused, and a review of metal-doped biochar for selective phosphate recovery and reuse is available [85]. For dyes, nano-magnetic *Tamarindus indica* seed biochar raised the malachite green capacity from 5.577 to 20.408 mg g^{-1} (and methyl blue from 3.055 to 3.326 mg g^{-1}), with four reuse tests passed [86]; magnetic chitosan–corn-straw biochar adsorbed amaranth dye [87]; and Fe_3O_4/ragweed biosorbent removed malachite green over five cycles [88]. Reviews of metal-ferrite/biochar nanocomposites cover dye adsorption and photocatalysis [89]. Hydrochar with embedded magnetic nanoparticles removed more than 95% of methylene blue but at a low capacity of 1.38 mg g^{-1} [25]. Magnetic biochar has also been applied to soils, where polluted-soil studies emphasize preparation methods, influencing factors and microbial response [19], and lead immobilization by phosphate-bearing biochar has been demonstrated [90].

Figure 12 compares the reported capacities across contaminant classes on a logarithmic scale.

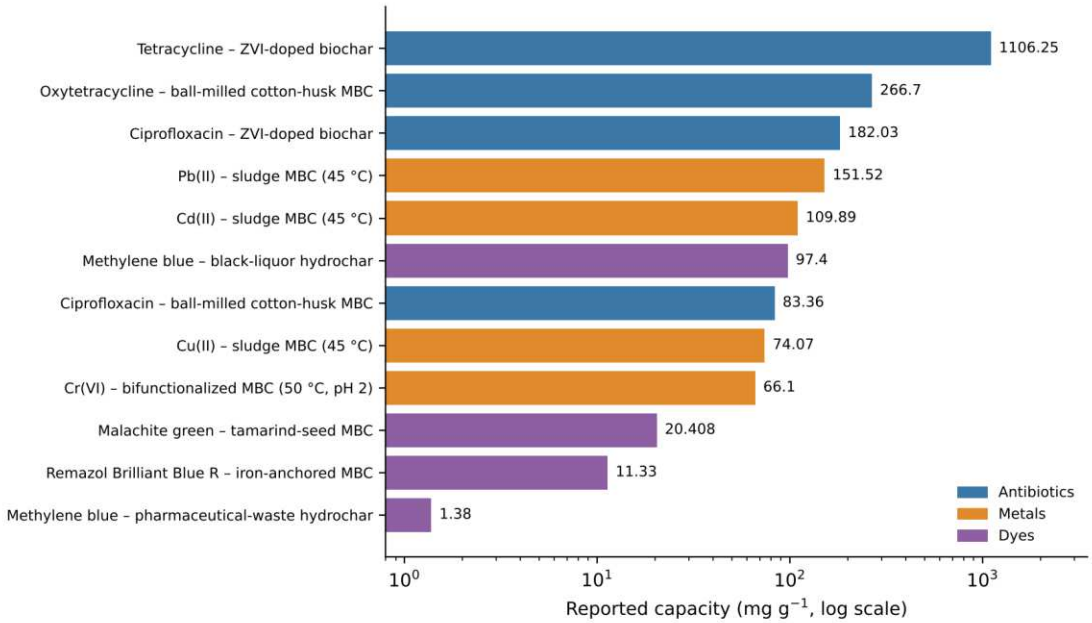

Figure 12. *Reported adsorption capacities of magnetic biochars and hydrochars by contaminant (logarithmic scale): ZVI-doped biochar [17], ball-milled cotton-husk biochar [60], sludge-derived biochar [42], black-liquor hydrochar [57], bifunctionalized biochar [39], tamarind-seed biochar [86], iron-anchored biochar [69] and pharmaceutical-waste hydrochar [25]. Values are as reported, at differing pH, temperature and dose.*

Table 8. *Adsorption systems for antibiotics, dyes and nutrients.*

Material	Target	Reported result / feature	Ref.
ZVI-doped biochar (K_2FeO_4/NaOH, 400 °C)	Tetracycline, ciprofloxacin	1106.25 and 182.03 mg g^{-1}; Ms 56.3 emu g^{-1}	[17]
Ball-milled magnetic cotton-husk biochar	Oxytetracycline, ciprofloxacin	266.7 and 83.36 mg g^{-1}; ethanol + ultrasound regeneration	[60]
Peanut-shell Fe_3O_4/BC	Tetracyclines	>85% over a wide pH range	[67]
Magnetite-functionalized biochar	Four sulfonamides	H-bond-controlled sorption	[66]
Mg–Fe LDH on magnetic biochar	Phosphate	Fe_3O_4-enabled recovery (2.63 emu g^{-1}); anion exchange	[37]
MgO-modified magnetic biochar (microwave)	Phosphate, Pb	One-step synthesis	[54]
Magnetic biochar, one-step vs electrochemical modification	Phosphate	Comparison of modification routes	[62]
Ball-milled S-doped nZVI@biochar	Phosphorus	Mechanochemical route	[33]
Nano-magnetic tamarind-seed biochar	Malachite green	20.408 vs 5.577 mg g^{-1} (unmodified)	[86]
Magnetic chitosan corn-straw biochar	Amaranth dye	Adsorption in aqueous solution	[87]
MNP-embedded hydrochar (pharmaceutical waste)	Methylene blue	>95% removal; 1.38 mg g^{-1}	[25]
Black-liquor magnetic hydrochar	Methylene blue	97.40 mg g^{-1}; 83.19% after five cycles	[57]
Iron-anchored magnetic biochar (FeO, $FeSO_4$, $FeCl_3$)	Remazol Brilliant Blue R	q_{max} 11.33 mg g^{-1}	[69]
Ca-rich β-cyclodextrin biochar (non-magnetic comparator)	Tetracycline	142.36→161.91 mg g^{-1} (25→45 °C); 84–86% retained after five cycles	[56]

7. Discussion

7.1 Regeneration, iron leaching and stability

Magnetic recovery is an advantage only if the sorbent can be reused. In the bifunctionalized system, removal fell to 61.12% after five adsorption–desorption cycles [39], whereas a calcium-rich β-cyclodextrin biochar retained about 84–86% of its capacity after five cycles [56], black-liquor hydrochar retained 83.19% [57], and iron-doped hydrochars were stable for six cycles with no detectable leaching [59]. Ethanol-plus-ultrasound regeneration and low iron leaching between pH 3 and 11 supported reuse of the ball-milled cotton-husk material [60]. Iron leaching, regeneration and environmental risk nevertheless remain unresolved for iron-modified biochar in general [5], and the ready oxidation of reduced iron makes storage and use conditions important [32]. Carbon coupling, as seen in graphitized kelp biochar, improves cycling stability [73].

7.2 Microbial interactions and soil applications

Magnetic biochar changes the electron transfer capacity of the material and thus microbial electron transfer [10], and reviews of its use in polluted soils stress microbial responses along with preparation and influencing factors [19]. MgO- and Fe_3O_4-loaded biochars have been tested for Cd passivation in soil together with maize growth [80]. Mineral-enriched biochars may add nutrient recovery and carbon dioxide removal benefits [20]. In soils magnetic recovery is not possible, so long-term iron fate and ecotoxicity, not recoverability, become the key issues.

7.3 Sustainability and life-cycle evidence

Life-cycle data for magnetic biochar are still sparse. A life cycle assessment of biodiesel production using impregnated magnetic biochar from palm kernel shell shows that such materials can be evaluated within full process chains [24], and hydrochar-embedded magnetic nanoparticles from waste compared favorably with co-precipitation and pyrolysis/gasification [25]. For a microwave-modified calcium-rich biochar, preparation generated 5.44 kg CO_2-eq per kg of adsorbent with electricity as the main hotspot [56]; although that adsorbent is not magnetic, the finding suggests that energy source and process time dominate burdens for thermally and microwave-assisted routes. Low-temperature carbothermal reduction [17] and one-pot syntheses [42] are therefore attractive on energy grounds, but their life-cycle benefits remain unquantified. Comparisons should be made per unit of pollutant removed rather than per mass of sorbent.

7.4 Data-driven design

Machine learning has been used to guide Mn-modified biochar preparation and predict Cd adsorption, with the best model reaching a test R^2 of 0.970 [21], and gradient boosting predicted tetracycline adsorption with a test R^2 of 0.9914, identifying initial concentration, dosage and contact time as key factors [56]. Reviews conclude that ML can predict adsorption of heavy metals with high accuracy and reduce experimental effort [22], that pyrolysis temperature dominates adsorption in SHAP analyses of engineered biochar, and that oxygen functional groups control redox behavior [23]. Six ML models have been compared for Pb^{2+} adsorption on biochars from tube-furnace and fluidized-bed pyrolysis [91], a transformer-based deep-learning model was trained on 1518 data points for heavy-metal uptake [92], and bibliometric analysis shows artificial neural networks and random forests as the commonest algorithms [93]. Studies of physical properties versus adsorption add to this evidence [94]. These models are limited by small, heterogeneous datasets for magnetic biochar specifically, which makes standardized reporting a prerequisite.

Figure 13 summarizes the reported reuse performance and machine-learning accuracy.

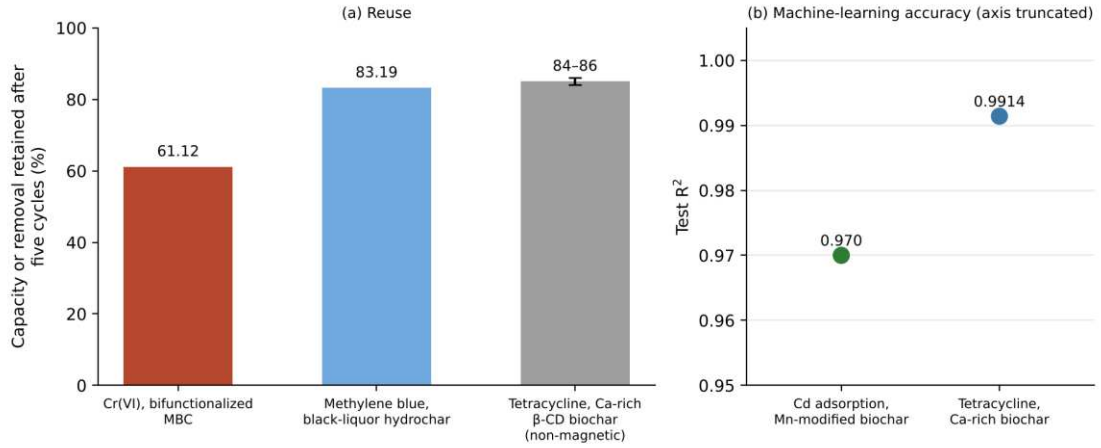

Figure 13. *(a) Capacity or removal retained after five cycles: bifunctionalized magnetic biochar [39], black-liquor magnetic hydrochar [57] and a calcium-rich β-cyclodextrin biochar (non-magnetic; 84–86%, plotted at 85%) [56]. (b) Test R^2 of machine-learning models for Cd adsorption on Mn-modified biochar [21] and tetracycline adsorption on a calcium-rich biochar [56]; note the truncated axis.*

7.5 Correlating processing, structure and performance parameters

Taken together, the reported values allow several quantitative correlations. (i) Temperature and capacity: raising the test temperature from 25 to 45 °C increased capacity by about 33% for Pb^{2+}, 9% for Cd^{2+} and 28% for Cu^{2+} on sludge-derived magnetic biochar [42], and by about 14% (142.36 to 161.91 mg g^{-1}) for tetracycline on the β-cyclodextrin biochar [56]; all are consistent with endothermic chemisorption. (ii) Preparation temperature and iron phase: Fe^0 was obtained at 400 °C with K_2FeO_4/NaOH, in contrast to the 600–1000 °C range studied for graphene-encapsulated Fe^0 [17, 38], and the lower-temperature route reached 56.3 emu g^{-1}. (iii) Iron loading and performance: optima occurred at 2% Fe for metals [42] and 10% Fe_3O_4 for chlorinated hydrocarbons [63], and iron activation lowered Pb(II) uptake by up to 86% in some biochars [41], so loading must be screened for each feedstock–target pair. (iv) Iron and radicals: EPFR content changed by factors of about +2.7, +2.8 and −2.9 depending on the precursor [78]. (v) Functionalization versus magnetization: ligand grafting added 27.63 percentage points of Cr(VI) removal against 10.95 for magnetization [39]. (vi) Capacity and magnetization: no consistent relationship was found across systems (Table 8, Figures 4 and 12). (vii) Reuse and design: retention after five cycles ranged from 61.12% [39] to about 83–86% [56, 57], which suggests that functional-group stability and carbon–iron coupling matter more for reuse than magnetization itself.

7.6 Critical synthesis: gaps and recommended actions

Table 9 lists the main knowledge gaps with recommended actions, and Figure 14 integrates them into a five-step roadmap.

Table 9. *Knowledge gaps and recommended actions for magnetic biochar interfaces.*

Gap	Why it matters	Recommended action	Ref.
Non-standard interfacial characterization	Prevents cross-study comparison of surface chemistry	Report Boehm/potentiometric titration, zeta potential, Fe speciation (XPS, Mössbauer, VSM)	[5, 39, 65, 79]
Single-solute, ultrapure-water tests	Overstates performance	Real water, competing ions, columns	[39, 81]
Mechanistic ambiguity (radical vs non-radical)	Scavenger evidence is non-selective	Combine EPR, probes and kinetics	[4, 27, 28, 34, 61]

Iron loading treated as monotonic benefit	Optimum or negative effects reported	Screen loading and Fe phase per feedstock	[41, 42, 63, 78]
Iron leaching and ecotoxicity under-reported	Secondary pollution risk	Leached-Fe and toxicity tests; carbon coupling	[5, 59, 60, 73]
Sparse life-cycle and techno-economic data	"Green" claims unquantified	Per-pollutant-removed LCA/TEA	[24, 25, 56]
Small datasets for machine learning	Limits predictive power	Community databases and consistent reporting	[21, 23, 56, 94]
Spent-sorbent fate	Metal-loaded material is waste	Recycle as catalyst or recover metals	[52]

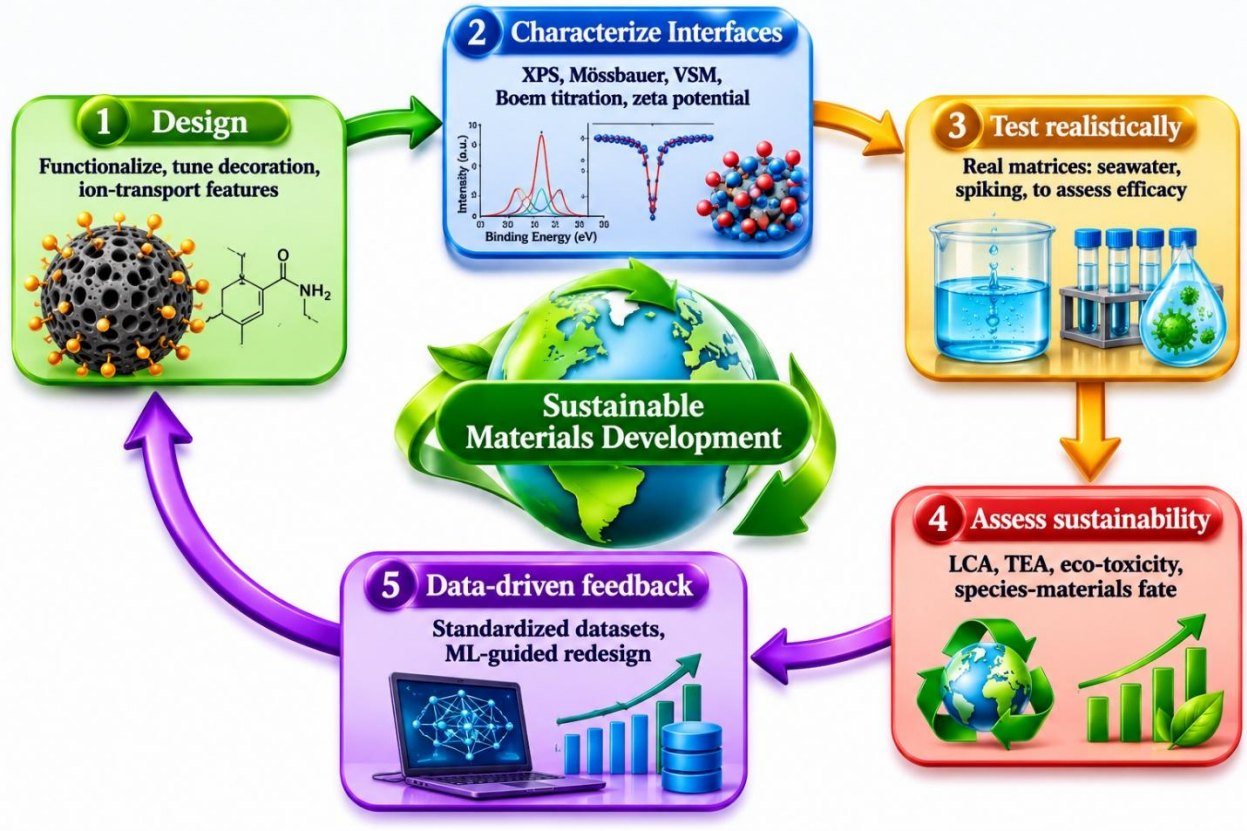

Figure 14. *Proposed five-step design and assessment roadmap for green magnetic biochar interfaces, integrating mild activation, interfacial characterization, realistic testing,*

sustainability assessment and data-driven feedback. Framework synthesized from refs [5, 21, 23–25, 56].

8. Challenges and Outlook

Four priorities emerge. First, interfacial characterization should become standard: surface charge, quantified functional groups and iron phase fractions need to be reported alongside surface area, because capacity gains can arise from reduction or precipitation rather than adsorption [5, 39, 65, 79]. Second, realistic testing in real water, columns and soil is essential, together with leaching and toxicity data [5, 19, 81]. Third, iron loading and phase must be optimized rather than maximized, given the optima and negative effects documented above [41, 42, 78]. Fourth, green claims require life-cycle and techno-economic evidence, with the functional unit expressed per amount of pollutant removed, and data-driven design needs curated, standardized datasets [23–25, 56]. Multifunctional and circular designs, such as spent sorbents reused as oxidant activators [52] or as nutrient carriers [37, 85], are promising directions.

9. Conclusions

Magnetic biochar interfaces can be tuned at three coupled levels: the solid–liquid surface chemistry, the carbon–iron junction and the pore–mineral architecture. The evidence reviewed here supports six conclusions, each tied to reported values.

First, green routes offer credible alternatives to hazardous reagents but trade off porosity, functional-group density, iron phase and stability. A 400 °C K_2FeO_4/NaOH carbothermal route produced Fe^0-doped biochar with a saturation magnetization of 56.3 emu g^{-1} and capacities of 1106.25 mg g^{-1} for tetracycline and 182.03 mg g^{-1} for ciprofloxacin, K_2CO_3 activation with ball milling reached 1638 m^2 g^{-1}, and black-liquor hydrochar reached 33.7 emu g^{-1} at 171.4 m^2 g^{-1} (Tables 2 and 3, Figures 3 and 4).

Second, functionalization usually adds more than magnetization alone: Cr(VI) removal rose from 61.42% to 72.37% on magnetization and to 100% on ligand grafting (Figure 10), and malachite green capacity increased from 5.577 to 20.408 mg g^{-1} on nano-magnetic modification [86].

Third, iron loading has an optimum and sometimes a penalty. Capacity peaked at 2% Fe in sludge-derived biochar and at 10% Fe_3O_4 for chlorinated hydrocarbons; magnetite activation reduced Pb(II) uptake by up to 86% in some biochars; and EPFR content rose from 3.33 to 9.11 × 10^{18} spins g^{-1} with iron in one hydrochar but fell from 7.95 to 2.78 × 10^{18} in another (Figure 7).

Fourth, in oxidation systems coexisting radical and non-radical pathways are the rule: about 56% radical and 44% non-radical in red-mud biochar, 56.3% Fe(IV) non-radical contribution in an iron/biochar persulfate system, and 99.74% phenol degradation by an oxidative-hydrothermal magnetic biochar (Table 7, Figure 9).

Fifth, durability is uneven. Removal retained after five cycles ranged from 61.12% to about 86%, some hydrochars showed no iron leaching over six cycles, and an electricity-dominated footprint of 5.44 kg CO_2-eq per kg was reported for a microwave-modified adsorbent.

Sixth, data-driven tools are promising (test R^2 of 0.970 and 0.9914 in two studies) but depend on standardized, larger datasets.

Rigorous interfacial characterization, optimization rather than maximization of iron loading, real-water validation and integrated life-cycle assessment are the most urgent needs for converting promising laboratory results into scalable, truly sustainable cleanup technologies (Table 9, Figure 14).

Declarations

Funding: The authors received no specific funding for this work.

Data availability: Not applicable.

Ethics approval and consent to participate: Not applicable.

Consent for publication: Not applicable.

Competing interests: The authors declare no competing interests.

Third-party material: Not applicable.

Data availability: No new data were generated for this review. Figures 1, 2, 3, 8, 9 and 14 are conceptual or qualitative syntheses; Figures 4–7 and 10–13 plot, or are calculated from, values reported in the cited sources.

References

1. Zhao Q, Xu T, Song X, Nie S, Choi S-E, Si C (2021) Preparation and application in water treatment of magnetic biochar. Front Bioeng Biotechnol 9:769667. https://doi.org/10.3389/fbioe.2021.769667

2. Sonowal S, Koch N, Sarma H, Prasad K, Prasad R (2023) A review on magnetic nanobiochar with their use in environmental remediation and high-value applications. J Nanomater 2023:4881952. https://doi.org/10.1155/2023/4881952
3. Kang K, Hu Y, Khan I, He S, Fetahi P (2023) Recent advances in the synthesis and application of magnetic biochar for wastewater treatment. Bioresour Technol 390:129786
4. Li Y, Zhang J, Cheng D, Guo W, Liu H, Guo A, Chen X, Wang Y, Ngo HH (2024) Magnetic biochar serves as adsorbents and catalyst supports for the removal of antibiotics from wastewater: a review. J Environ Manage 366:121872. https://doi.org/10.1016/j.jenvman.2024.121872
5. Zhang Y, Chen H, Islam S (2025) Advances in biochar modification for environmental remediation with emphasis on iron functionalization. Biochar X 1:e009. https://doi.org/10.48130/bchax-0025-0010
6. Lohan, D., Jain, R., Srivastava, A., Dutta, S., Mohan, D., & Sharma, R.K. (2023). Surface Engineering approaches for the design of magnetic biochar-composites for removal of heavy metals: A comprehensive review. J Environ Chem Eng (2023) https://doi.org/10.1016/j.jece.2023.111448
7. Kong F, Liu J, Xiang Z, Fan W, Liu J, Wang J, Wang Y, Wang L, Xi B. Degradation of Water Pollutants by Biochar Combined with Advanced Oxidation: A Systematic Review. Water. 2024; 16(6):875. https://doi.org/10.3390/w16060875
8. Zhang R, Zhang R, Zimmerman AR, Wang H, Gao B (2023) Applications, impacts, and management of biochar persistent free radicals: a review. Environ Pollut 327:121543. https://doi.org/10.1016/j.envpol.2023.121543
9. Liu X, Chen Z, Lu S, Shi X, Qu F, Cheng D, Wei W, Shon HK, Ni BJ. Persistent free radicals on biochar for its catalytic capability: A review. Water Res. 2024 Feb 15;250:120999. doi: 10.1016/j.watres.2023.120999.
10. An T, Chang Y, Xie J, Cao Q, Liu Y, Chen C (2022) Deciphering physicochemical properties and enhanced microbial electron transfer capacity by magnetic biochar. Bioresour Technol 363:127894
11. Amusat SO, Kebede TG, Dube S, Nindi MM (2021) Ball-milling synthesis of biochar and biochar-based nanocomposites and prospects for removal of emerging contaminants: a review. J Water Process Eng 41:101993

12. Zhang N, Reguyal F, Sarmah AK (2024) Effect of iron nanoparticles on chromium adsorption in aqueous solution using magnetic biochar: a site energy distribution analysis. Environ Pollut 123593. https://doi.org/10.1016/j.envpol.2024.123593
13. Zhang N, Reguyal F, et al. (2023) A green approach of biochar-supported magnetic nanocomposites from white tea waste: production, characterization and plausible synthesis mechanisms. Sci Total Environ. https://doi.org/10.1016/j.scitotenv.2023.163923
14. Tong et al. (2023) Persulfate activation by Fe_3O_4-doped biochar synthesized from Fenton sludge and sewage sludge for enhanced 1-H-1,2,4-triazole degradation. Chem Eng J 461:142075. https://doi.org/10.1016/j.cej.2023.142075
15. Wu Q, Zhang Y, Liu H, Liu H, Tao J, et al. (2022) Fe_xN produced in pharmaceutical sludge biochar by endogenous Fe and exogenous N doping to enhance peroxymonosulfate activation for levofloxacin degradation. Water Res 224:119022
16. Sun A, Liang Y, He K, Pan Q, Luo S, Liu X, Jiang H, Li J (2024) Oxidative hydrothermal carbonization to fabricate versatile magnetic biochar for Fenton-like degradation of phenolic compounds. J Environ Chem Eng 12(6):114822. https://doi.org/10.1016/j.jece.2024.114822
17. Jin, Y., Zheng, C., Sun, A., Jiang, H., Xiao, Y., Li, J., ... & Li, J. (2025). Synergistic Effect of Potassium Ferrate and Sodium Hydroxide in Lowering Carbothermal Reduction Temperature: Preparation of Magnetic Zero-Valent Iron-Doped Biochar for Antibiotic Removal. Processes, 13(9), 2806. https://doi.org/10.3390/pr13092806
18. † Li M, Wang P, Huang C, Liu Y, Liu S, Zhang K, Cao J, Tan X, Liu S. Effect of dissolved humic acids and coated humic acids on tetracycline removal by K_2CO_3-activated magnetic biochar [journal and year to be verified]
19. El-Hussein, A., Ioanid, A., Surour, A. A., Ashry, M. M., Sanad, M. N., Farouz, M., ... & Abd El-Sadek, M. S. (2026). Review of Preparation, Application, and Microbiological Reaction of Magnetic Biochar for Heavy Metal Removal from Polluted Soils. Chemistry, 8(4), 47.https://doi.org/10.3390/chemistry8040047
20. Buss W, Wurzer C, Manning DA, Rohling EJ, Borevitz J, Mašek O (2022) Mineral-enriched biochar delivers enhanced nutrient recovery and carbon dioxide removal. Commun Earth Environ 3:67

21. Wang W, Zhou Z, Wang J, et al. (2026) Data-driven machine learning models for guiding the preparation of Mn-modified biochar and predicting Cd adsorption. Adv Compos Hybrid Mater. https://doi.org/10.1007/s42114-026-01997-z
22. Chen, M. W., Chang, M. S., Mao, Y., Hu, S., & Kung, C. C. (2023). Machine learning in the evaluation and prediction models of biochar application: A review. Sci Prog 106(1):368504221148842 (2023). https://doi.org/10.1177/00368504221148842
23. Ge Y, Ying K, Yu G, Ali MU, Idris AM, Shahab A, Ullah H (2025) A systematic review on machine learning-aided design of engineered biochar for soil and water contaminant removal. Front Soil Sci 5:1623083. https://doi.org/10.3389/fsoil.2025.1623083
24. Anak Erison AE, Tan YH, Mubarak NM, Kansedo J, Khalid M, Abdullah MO, Ghasemi M (2022) Life cycle assessment of biodiesel production by using impregnated magnetic biochar derived from waste palm kernel shell. Environ Res 214:114149
25. Yunus AI, Darko SA, Chen Y, Bozeman JF III (2025) Facile fabrication of magnetite (Fe3O4) nanoparticles by hydrothermal carbonization of waste iron supplements. RSC Sustain 3:3530. https://doi.org/10.1039/d5su00312a
26. Foong SY, Chan YH, Chin BLF, Lock SSM, Yee CY, Yiin CL, Peng W, Lam SS (2022) Production of biochar from rice straw and its application for wastewater remediation: an overview. Bioresour Technol 360:127588
27. Wang Q, Shi Y, Lv S, Liang Y, Xiao P (2021) Peroxymonosulfate activation by tea residue biochar loaded with Fe_3O_4 for the degradation of tetracycline hydrochloride: performance and reaction mechanism. RSC Adv 11:18525–18538. https://doi.org/10.1039/d1ra01640g
28. Wang, J., Zhou, R., Wang, L., Guan, T., Li, Z., & Zhao, X. (2026). Red mud biochar as an efficient peroxymonosulfate activator for tetracycline degradation: Synergistic radical/non-radical mechanisms and process optimization for sustainable waste valorization. Global NEST Journal, 28(4), 1-17. https://doi.org/10.30955/gnj.08393
29. Shamsuyeva M, Endres H-J, Papenbrock J, Behrens P, Weichgrebe D, et al. (2023) Physico-chemical characterization of walnut shell biochar. Clean Technol Environ Policy 25:2727–2746. https://doi.org/10.1007/s10098-023-02525-z
30. Xue H, Deng L, Kang D, Zhao Y, Zhang X, Liu Y, Chen H, Ngo HH, Guo W (2024) Advanced biochar-based materials for specific antibiotics removal from hospital

wastewater via adsorption and oxidative degradation. J Environ Chem Eng. https://doi.org/10.1016/j.jece.2024.114275

31. Shi X, Yang W, Li J, Yao Z (2024) The application of biochar as heavy metals adsorbent: the preparation, mechanism, and perspectives. Int J Environ Res 18:41. https://doi.org/10.1007/s41742-024-00592-8
32. Kızılbey K, Köprülü EN, Temür H, Canım Ateş S, Özer S. Magnetic and Biomedical Properties of Iron Nanoparticles Synthesized Using Vitex agnus-castus Extract. Materials (Basel). 2024 Dec 11;17(24):6064. doi: 10.3390/ma17246064. PMID: 39769664; PMCID: PMC11677412.
33. Ai D, Wei T, Meng Y, Chen X, Wang B. Ball milling sulfur-doped nano zero-valent iron @biochar composite for the efficient removal of phosphorus from water: Performance and mechanisms. Bioresour Technol. 2022 Aug;357:127316. doi: 10.1016/j.biortech.2022.127316. Epub 2022 May 18. PMID: 35597516.
34. Xu et al. (2022) Activation of peroxymonosulfate by $MnFe_2O_4$@BC composite for bisphenol A degradation: the coexisting of free-radical and non-radical pathways. Chem Eng J 442:136250. https://doi.org/10.1016/j.cej.2022.136250
35. Guo Y, Yan L, Li X, Yan T, Song W, et al. (2021) Goethite/biochar-activated peroxymonosulfate enhances tetracycline degradation: inherent roles of radical and non-radical processes. Sci Total Environ 783:147102
36. Wang et al. (2023) Enhanced mechanism of copper doping in magnetic biochar for peroxymonosulfate activation and sulfamethoxazole degradation. J Hazard Mater 458:132002. https://doi.org/10.1016/j.jhazmat.2023.132002
37. Li X, Xin L, Peng Y, Zhang S, Guan D, Song J. Sustainable Phosphate Remediation via Hierarchical Mg-Fe Layered Double Hydroxides on Magnetic Biochar from Agricultural Waste. Magnetochemistry. 2025; 11(4):27. https://doi.org/10.3390/magnetochemistry11040027
38. Karunaratne, T.N., Nayanathara, R.M.O., Navarathna, C.M. et al. Pyrolytic synthesis of graphene-encapsulated zero-valent iron nanoparticles supported on biochar for heavy metal removal. Biochar 4, 70 (2022). https://doi.org/10.1007/s42773-022-00196-5
39. Cui X, Wang J, Zhao Q, Li C, Huang J, Hu X, Li J, Li M. Application of a Novel Bifunctionalized Magnetic Biochar to Remove Cr(VI) from Wastewater: Performance

and Mechanism. Separations. 2023; 10(6):358. https://doi.org/10.3390/separations10060358

40. Lopez-Tenllado et al. (2021) Modification of biochar with high-energy ball milling: development of porosity and surface acid functional groups. Bioresour Technol Rep 15:100704. https://doi.org/10.1016/j.biteb.2021.100704
41. Chen, N., Kwak, J., Nzediegwu, C. et al. Feedstock type and pyrolysis temperature drive lead(II) adsorption on magnetite-impregnated biochar in aqueous solutions. Int. J. Environ. Sci. Technol. 22, 6999–7012 (2025). https://doi.org/10.1007/s13762-024-06106-5
42. Tian J, Guo K, Sun Y, Lin R, Chen T, Zhang B, Liu Y, Yang T. Solvent-Free Synthesis of Magnetic Sewage Sludge-Derived Biochar for Heavy Metal Removal from Wastewater. International Journal of Environmental Research and Public Health. 2023; 20(1):155. https://doi.org/10.3390/ijerph20010155
43. Maniarasu R, et al. (2022) Biomass-based activated carbon for CO_2 adsorption: a review. Energy Environ 34(4). https://doi.org/10.1177/0958305X221093465
44. Wu W, Wu C, Zhang G, Liu J, Li Y, Li G (2023) Synthesis and characterization of magnetic K_2CO_3-activated carbon produced from bamboo shoot for the adsorption of Rhodamine B and CO_2 capture. Fuel 332:126107. DOI: 10.1016/j.fuel.2022.126107.
45. Miaomiao Zhang, Pengwei Li, Dong Guo, Ziheng Zhao, Weisheng Feng, Zhijuan Zhang; Highly Efficient Adsorption of Norfloxacin by Low-Cost Biochar: Performance, Mechanisms, and Machine Learning-Assisted Understanding. ACS Omega 16 July 2024; 9 (28): 30813–30825. https://doi.org/10.1021/acsomega.4c03496
46. Zhang H, Wu Z, Shi Q, Khan A, et al. (2023) Fabrication and characterization of magnetic eucalyptus carbon for efficient Cr(VI) removal in aqueous solution and its mechanisms. Arab J Chem 09 2023 :16;105047. doi: 10.1016/j.arabjc.2023.105047
47. Sun Y, Zheng L, Zheng X, Xiao D, Yang Y, Zhang Z, Ai B and Sheng Z (2022) Adsorption of Sulfonamides in Aqueous Solution on Reusable Coconut-Shell Biochar Modified by Alkaline Activation and Magnetization. Front. Chem. 9:814647. doi: 10.3389/fchem.2021.814647

48. Wang Q, Yue Y, Liu W, Liu Q, Song Y, Ge C, Ma H. Removal Performance of KOH-Modified Biochar from Tropical Biomass on Tetracycline and Cr(VI). Materials. 2023; 16(11):3994. https://doi.org/10.3390/ma16113994
49. Ren H, Su M, Hou Y, Liu Z (2023) Activated carbon with ultrahigh specific surface derived from bamboo shoot shell through K_2FeO_4 oxidative pyrolysis for adsorption of methylene blue. Molecules 28:3410. https://doi.org/10.3390/molecules28083410
50. Ghoohestani E, Samari F, Homaei A, Yousefinejad S (2024) A facile strategy for preparation of Fe_3O_4 magnetic nanoparticles using *Cordia myxa* leaf extract and investigating its adsorption activity in dye removal. *Sci Rep* **14:84**. https://doi.org/10.1038/s41598-023-50550-1
51. Mohamed Mohamed Gaber, Arafat Toghan, Hassan Shokry, Mahmoud Samy; Efficient oxidative degradation of organic pollutants in real industrial effluents using a green-synthesized magnetite supported on biochar catalyst. RSC Adv. 2025; 15 (38): 31522–31538. https://doi.org/10.1039/d5ra04070a
52. Pan J, Gao B, Duan P, Guo K, Xu X, et al. (2021) Recycling exhausted magnetic biochar with adsorbed Cu^{2+} as a cost-effective permonosulfate activator for norfloxacin degradation: Cu contribution and mechanism. J Hazard Mater 413:125413
53. Qu et al. (2021) Magnetic porous biochar with high specific surface area derived from microwave-assisted hydrothermal and pyrolysis treatments of water hyacinth for Cr(VI) and tetracycline adsorption from water. Bioresour Technol 340:125692. DOI: 10.1016/j.biortech.2021.125692
54. Wei, S., Tao, Y., Ma, M., Tong, W., Bi, F., Wang, L., ... & Zhang, Y. (2025). One-step microwave-assisted synthesis of MgO-modified magnetic biochar for enhanced removal of lead and phosphate from wastewater: Performance and mechanisms. Separation and Purification Technology, 354, 128936. https://doi.org/10.1016/j.seppur.2024.128936
55. Nassar AE, El-Aswar EI, Rizk SA, Gaber SES, Jahin HS (2023) Microwave-assisted hydrothermal preparation of magnetic hydrochar for the removal of organophosphorus insecticides from aqueous solutions. Sep Purif Technol 306(Part A):122569. DOI: 10.1016/j.seppur.2022.122569
56. Liu C, Crini G, Bello-Mendoza R, Wilson LD, Jawad AH, Balasubramanian P, Nguyen XC, Zheng Q, Li F (2026) Microwave-assisted β-cyclodextrin modified calcium-rich

biochar for tetracycline removal from wastewater: mechanistic, machine learning, density functional theory calculations and life cycle assessment. Biochar 8:124. https://doi.org/10.1007/s42773-026-00640-w

57. Nguyen B.N., Nguyen N.H., Phan P.T., Phama T.C., Nguyen T.D., Phame N.S., Nguyen A.Q., 2022, Hydrothermal Conversion of Black Liquor to Magnetic Hydrochar and Its Potential for Methylene Blue Removal, Chemical Engineering Transactions, 96, 469-474. https://doi.org/10.3303/CET2296079
58. Saygili GA, Saygili H (2022) Fabrication of a magnetic hydrochar composite via an in situ one-pot hydrocarbonization strategy for efficient herbicide removal. Diam Relat Mater 128:109302. doi. 10.1016/j.diamond.2022.109302
59. Dasgupta T, Rajput H, Perera P, Sun X, He Q. 2025. Sustainable carbon materials for magnetic adsorbent-based pentachlorophenol removal from wastewater. Sustainable Carbon Materials 1: e003 doi: 10.48130/scm-0025-0003
60. Chen, C., Yang, F., Ma, Y. et al. Ball milling boosted magnetic cotton husk-derived biochar adsorptive removal of oxytetracycline and ciprofloxacin from water. Carbon Res. 3, 63 (2024). https://doi.org/10.1007/s44246-024-00146-9
61. Yu Y, Guo H, Zhong Z, Wang A, Xiang M, Xu S, Dong C, Chang Z (2022) Fe_3O_4 loaded on ball milling biochar enhanced bisphenol A removal by activating persulfate: performance and activating mechanism. J Environ Manage 115661. https://doi.org/10.1016/j.jenvman.2022.115661
62. Mei C, Wang L, Tao W. Characterization of Magnetic Biochar Modified Using the One-Step and Electrochemical Methods and Its Impact on Phosphate Adsorption. Materials. 2023; 16(22):7092. https://doi.org/10.3390/ma16227092
63. Zhang F, Li Z, Dou X, Liu Z, Xie Y, Liu J, Zhang S. Pore-Engineered Magnetic Biochar: Optimizing Pyrolysis and Fe3O4 Loading for Targeted Chlorinated Aliphatic Hydrocarbon (CAH) Adsorption. Separations. 2025; 12(10):260. https://doi.org/10.3390/separations12100260
64. Guo et al. (2023) Mechanism of efficient magnetic biochar for typical aqueous organic contaminant combined-adsorption removal. Fuel Process Technol 247:107795. https://doi.org/10.1016/j.fuproc.2023.107795

65. Wood R, Mašek O, Erastova V.Developing a molecular-level understanding of biochar materials using public characterization data. Cell Reports Physical Science, 2024; 5. DOI: 10.1016/j.xcrp.2024.102036
66. Bai S, Zhou Y, Qian M, Xia J, Sun Z, Wang Y, Huang X, Zhu S (2023) Mechanistic insights to sorptive removal of four sulfonamide antibiotics from water using magnetite-functionalized biochar. Biochar 5. https://doi.org/10.1007/s42773-023-00283-1
67. Zhang Q, Zhang H, Hua Q, Yuan C, et al. (2024) Effect on the adsorption performance and mechanism of antibiotics tetracyclines by the magnetic biochar used peanut shells as raw materials. Mater Res Express
68. Singh V, Pant N, Sharma RK, Padalia D, Rawat PS, Goswami R, Singh P, Kumar A, Bhandari P, Tabish A, et al. Adsorption Studies of Pb(II) and Cd(II) Heavy Metal Ions from Aqueous Solutions Using a Magnetic Biochar Composite Material. Separations. 2023; 10(7):389. https://doi.org/10.3390/separations10070389
69. Chakma S, Sutradhar S, Rakshit SK, Fatehi P, Kang K (2025) Study on iron anchoring methods for magnetic biochar: characterization, functional mechanism, and RBBR dye removal. Can J Chem Eng
70. Tian L, Li H, Chang Z, et al. (2023) Biochar modification to enhance arsenic removal from water: a review. Environ Geochem Health 45(6):2763–2778. https://doi.org/10.1007/s10653-022-01462-y
71. Zhang K, Yi Y, Fang Z (2023) Remediation of cadmium or arsenic contaminated water and soil by modified biochar: a review. Chemosphere 311:136914. https://doi.org/10.1016/j.chemosphere.2022.136914
72. Chatzimichailidou S, Xanthopoulou M, Tolkou AK, et al. (2023) Biochar derived from rice by-products for arsenic and chromium removal by adsorption: a review. J Compos Sci 7(2):59. https://doi.org/10.3390/jcs7020059
73. Fangke Yu, Yan Song, Yueping Guo, Jing Yang; Degradation of tetracycline by persulfate oxidation promoted by iron-modified biochar. New J. Chem. 2022; 46 (46): 22459–22468. https://doi.org/10.1039/d2nj03348h
74. Diao et al. (2023) Efficient adsorption of a sulfonamide antibiotic in aqueous solutions with N-doped magnetic biochar: performance, mechanism, and reusability. ACS Omega 8:879. https://doi.org/10.1021/acsomega.2c06234

75. Deng H, He H, Li W, Abbas T, Liu Z (2022) Characterization of amphoteric bentonite-loaded magnetic biochar and its adsorption properties for Cu^{2+} and tetracycline. PeerJ 10:e13030. https://doi.org/10.7717/peerj.13030
76. Zhu et al. (2022) Efficient tetracycline degradation via peroxymonosulfate activation by magnetic Co/N co-doped biochar: emphasizing the important role of biochar graphitization. Chem Eng J 450:138428. https://doi.org/10.1016/j.cej.2022.138428
77. Tang Y, Dou J, Lu Z, Xu J, He Y. Accelerating Fe2+/Fe3+ cycle via biochar to improve catalytic degradation efficiency of the Fe3+/persulfate oxidation. Environ Pollut. 2023 Jan 1;316(Pt 2):120669. doi: 10.1016/j.envpol.2022.120669. Epub 2022 Nov 14. PMID: 36395909.
78. Zhang, C., Jiang, Z., Sun, W. et al. Activating Fenton-like reaction by hydrochars containing persistent free radicals derived from various pomelo peel components. Biochar 6, 69 (2024). https://doi.org/10.1007/s42773-024-00362-x
79. Choi, K., Lee, S. Y., Kim, H., Lee, K. B., Choi, J. W., & Jung, K. W. (2022). Mechanistic insights into the simultaneous removal of As (V) and Cr (VI) oxyanions by a novel hierarchical corolla-like MnO2-decorated porous magnetic biochar composite: A combined experimental and density functional theory study. Applied Surface Science, 578, 151991. https://doi.org/10.1016/j.apsusc.2021.151991
80. Ding H, Liu J, Li Q, Liu Z, Xia K, Hu L, Wu X, Yan Q (2023) Highly effective adsorption and passivation of Cd from wastewater and soil by MgO- and Fe_3O_4-loaded biochar nanocomposites. Front Environ Sci 11:1239842. https://doi.org/10.3389/fenvs.2023.1239842
81. Ahmed Khan B, Ahmad M, Bolan N, Farooqi A, Iqbal S, Mickan B, Solaiman ZM, Siddique KHM. A mechanistic approach to arsenic adsorption and immobilization in aqueous solution, groundwater, and contaminated paddy soil using pine-cone magnetic biochar. Environ Res. 2024 Mar 15;245:117922. doi: 10.1016/j.envres.2023.117922.
82. Jin et al. (2023) Competitive adsorption of sulfamethoxazole and bisphenol A on magnetic biochar: mechanism and site energy distribution. Environ Pollut 329:121662. https://doi.org/10.1016/j.envpol.2023.121662

83. Du et al. (2023) A review of antibiotics and antibiotic resistance genes (ARGs) adsorption by biochar and modified biochar in water. Sci Total Environ 858:159815. https://doi.org/10.1016/j.scitotenv.2022.159815
84. Masud et al. (2023) Fe-doped kelp biochar-assisted peroxymonosulfate activation for ciprofloxacin degradation: multiple active site-triggered radical and non-radical mechanisms. Chem Eng J 471:144519. https://doi.org/10.1016/j.cej.2023.144519
85. Qu et al. (2024) Metal-doped biochar for selective recovery and reuse of phosphate from water: modification design, removal mechanism, and reutilization strategy. Bioresour Technol 407:131075. https://doi.org/10.1016/j.biortech.2024.131075
86. Bayram O, Moral E, Köksal E, Göde F, Pehlivan E (2023) Removal of methyl blue and malachite green from water using biodegradable magnetic Tamarindus indica fruit seed biochar: characterization, equilibrium study, modelling and thermodynamics. Sustain Chem Environ 3:100023. https://doi.org/10.1016/j.scenv.2023.100023
87. Wang F, Li L, Iqbal J, Yang Z, Du Y (2022) Preparation of magnetic chitosan corn straw biochar and its application in adsorption of amaranth dye in aqueous solution. Int J Biol Macromol 199:234. https://doi.org/10.1016/j.ijbiomac.2021.12.195
88. Nedić N, Tadić T, Marković B, Nastasović A, Popović A, Bulatović S. Eco-Friendly Green Approach to the Biosorption of Hazardous Dyes from Aqueous Solution on Ragweed (Ambrosia artemisiifolia) Biomass. Separations. 2024; 11(11):310. https://doi.org/10.3390/separations11110310
89. Dhila, H.H., Bhapkar, A.R., & Bhame, S. (2025). Metal Ferrite/Biochar Nanocomposites for Dye Pollutant Removal: Insights into Adsorption and Photocatalytic Strategies. ChemistrySelect (2025). https://doi.org/10.1002/slct.202504007
90. Beatrice A, Varco JJ, Dygert A, Atsar FS, Solomon S, Thirumalai RVKG, Pittman CU Jr, Mlsna T (2022) Lead immobilization in simulated polluted soil by Douglas fir biochar-supported phosphate. Chemosphere 292:133355. https://doi.org/10.1016/j.chemosphere.2021.133355
91. Huang W, Wang L, Zhu J, Dong L, Hu H, Yao H, Wang L, Lin Z. Application of machine learning in prediction of Pb^{2+} adsorption of biochar prepared by tube furnace and fluidized bed. Environ Sci Pollut Res Int. 2024 Apr;31(18):27286-27303. doi: 10.1007/s11356-024-32951-5.

92. Jaffari ZH, Abbas A, Kim CM, Shin J, Kwak J, Son C, Lee YG, Kim S, Chon K, Cho KH. Transformer-based deep learning models for adsorption capacity prediction of heavy metal ions toward biochar-based adsorbents. J Hazard Mater. 2024 Jan 15;462:132773. doi: 10.1016/j.jhazmat.2023.132773.
93. Oral B, Coşgun A, Günay ME, Yıldırım R. Machine learning-based exploration of biochar for environmental management and remediation. J Environ Manage. 2024 Jun;360:121162. doi: 10.1016/j.jenvman.2024.121162.
94. Al-Zyoud, M., Mostafa, S. A., Khersan, I., Gowrishankar, J., Sahu, P. K., Singla, S., ... & Sherzod, S. (2026). Effects of physical properties on the heavy metal adsorption of biochar via a robust approach. Curr Res Biotechnol 11:100367 (2026).